OXFORD

Cerebral Cortex, 2022, 1–19
https://doi.org/10.1093/cercor/bhac355
Original Article

A microcircuit model involving parvalbumin, somatostatin, and vasoactive intestinal polypeptide inhibitory interneurons for the modulation of neuronal oscillation during visual processing

Nobuhiko Wagatsuma [1], Sou Nobukawa[2,3], Tomoki Fukai[4]

[1]Faculty of Science, Toho University, 2-2-1 Miyama, Funabashi, Chiba 274-8510, Japan,
[2]Department of Computer Science, Chiba Institute of Technology, 2-17-1 Tsudanuma, Narashino, Chiba 275-0016, Japan,
[3]Department of Preventive Intervention for Psychiatric Disorders, National Institute of Mental Health, National Center of Neurology and Psychiatry, 4-1-1 Ogawa-Higashi, Kodaira, Tokyo 187-8502, Japan,
[4]Neural Coding and Brain Computing Unit, Okinawa Institute of Science and Technology Graduate University, 1919-1 Tancha, Onna-son, Kunigami-gun, Okinawa 904-0495, Japan
*Corresponding author: Faculty of Science, Toho University, Miyama 2-2-1, Funabashi, Chiba 274-8510, Japan. Email: nwagatsuma@is.sci.toho-u.ac.jp

Various subtypes of inhibitory interneurons contact one another to organize cortical networks. Most cortical inhibitory interneurons express 1 of 3 genes: parvalbumin (PV), somatostatin (SOM), or vasoactive intestinal polypeptide (VIP). This diversity of inhibition allows the flexible regulation of neuronal responses within and between cortical areas. However, the exact roles of these interneuron subtypes and of excitatory pyramidal (Pyr) neurons in regulating neuronal network activity and establishing perception (via interactions between feedforward sensory and feedback attentional signals) remain largely unknown. To explore the regulatory roles of distinct neuronal types in cortical computation, we developed a computational microcircuit model with biologically plausible visual cortex layers 2/3 that combined Pyr neurons and the 3 inhibitory interneuron subtypes to generate network activity. In simulations with our model, inhibitory signals from PV and SOM neurons preferentially induced neuronal firing at gamma (30–80 Hz) and beta (20–30 Hz) frequencies, respectively, in agreement with observed physiological results. Furthermore, our model indicated that rapid inhibition from VIP to SOM subtypes underlies marked attentional modulation for low-gamma frequency (30–50 Hz) in Pyr neuron responses. Our results suggest the distinct but cooperative roles of inhibitory interneuron subtypes in the establishment of visual perception.

Key words: computational model; inhibitory interneuron subtypes; neuronal oscillation; primary visual cortex; selective attention.

Introduction

In cortical microcircuits of the primary visual area (V1), interactions between feedforward visual inputs—projected from the retina—and feedback attentional signals are fundamental for establishing perception and for understanding the external world. One of the most critical neural circuits for receiving and integrating signals exists in the superficial layers (2 and 3) and consists of excitatory pyramidal (Pyr) neurons and distinct subtypes of inhibitory interneurons expressing 1 of 3 genes: parvalbumin (PV), somatostatin (SOM), or vasoactive intestinal polypeptide (VIP) (Zhang et al. 2014; Neske et al. 2015; Mardinly et al. 2016; Cardin 2018). Interactions among these neuronal populations regulate and modulate not only neural activity but also the oscillatory rhythms of neuronal networks. However, the detailed roles of these interneuron subtypes for processing feedforward inputs (representing visual stimuli) and feedback signals (mediating selective attention) and for establishing visual perception remain largely unknown. A clarification of the microcircuit structure based on Pyr neurons and these 3 interneuron subtypes will provide important insights into the mechanisms of oscillatory activity generation in the V1.

Analyses of neuronal dynamics and synchronized activity can provide insights into the cortical mechanisms of sensory processing and perception (Aertsen and Arndt 1993; Pillow et al. 2008; Martin and von der Heydt 2015; Yatsenko et al. 2015). Neuronal populations in a range of cortical areas are synchronized; oscillations involve multiple timescales to facilitate sensory processing and perform attentional modulation (Uhlhaas and Singer 2010; Cardin 2018). Visual attention to a target stimulus relevant to the experimental task improves behavioral performance measures (such as reaction time and accuracy) in animals and enhances the amplitude of neuronal oscillations in a specific frequency range, which implies that selective frequency modulation underlies the establishment of perception by rendering relevant input and neuronal communication effective (Womelsdorf et al. 2006; Bosman et al. 2012; Rohenkohl et al. 2018). Notably, physiological studies have demonstrated that distinct subtypes of local inhibitory interneurons exert differential and coordinated regulation of rhythmic activity in the cortex (Chen et al. 2017; Veit et al. 2017; Jang et al. 2020). A computational and theoretical model approach can be used to investigate the detailed structure of neuronal microcircuits that drive the physiologically observed functions of inhibitory interneuron subtypes.

Computational models and simulations are powerful tools for studying the complex structures and networks of cortical microcircuits which are organized by interactions among various types

Received: April 3, 2022. **Revised:** August 6, 2022. **Accepted:** August 8, 2022
© The Author(s) 2022. Published by Oxford University Press. All rights reserved. For permissions, please e-mail: journals.permissions@oup.com
This is an Open Access article distributed under the terms of the Creative Commons Attribution Non-Commercial License (https://creativecommons.org/licenses/by-nc/4.0/), which permits non-commercial re-use, distribution, and reproduction in any medium, provided the original work is properly cited. For commercial re-use, please contact journals.permissions@oup.com

of neurons. For example, neural network models that include different types of neural connections—such as feedforward, recurrent, horizontal, and feedback connections—have elucidated the mechanisms and functions of fast oscillatory activity in layers 2/3 of the V1 (Jia et al. 2013; Han, Shapley, et al. 2021a). Furthermore, the structures of cortical microcircuits—including a variety of neuronal classes—have been theoretically and computationally investigated to aid our understanding of the neural mechanisms of sensory processing (Lee et al. 2017, 2018; Lee and Mihalas 2017; Wilmes and Clopath 2019); these models were developed by integrating physiological knowledge about the various classes and subtypes of neurons in the cortex (Pfeffer et al. 2013; Zhang et al. 2014; Neske et al. 2015; Mardinly et al. 2016). Another computational study numerically demonstrated the contribution of a long-tailed distribution of synaptic strengths in recurrent connections between excitatory Pyr neurons to the generation of stochastic resonance and noisy internal brain states (Teramae et al. 2012; Nobukawa, Nishimura, et al. 2021a; Nobukawa, Wagatsuma, et al. 2021b). Analyses of such a model based on the integration of recent physiological and computational research may provide valuable insights into the mechanisms of complex interactions between feedforward sensory inputs and feedback attentional signals within the cortical microcircuit.

In the present study, we integrated much of the current knowledge on cortical microcircuitry to develop a network model with a biologically plausible structure of layers 2/3 in the V1; the model consisted of excitatory Pyr neurons and the 3 subtypes (PV, SOM, and VIP) of inhibitory interneurons (Fig. 1(a)). This microcircuit model represented the functional unit of layers 2/3 in the V1 when processing a specific visual feature projected onto its receptive field, which is similar to a previous computational study (Potjans and Diesmann 2014). These neuronal populations cooperate and interact with one another to process feedforward inputs (representing visual stimuli) and feedback signals (mediating selective attention) and to regulate synchronized oscillatory activation. In our microcircuit model, Pyr neurons were recurrently connected based on a long-tailed distribution in their synaptic weights (Song et al. 2005; Lefort et al. 2009; Teramae et al. 2012; Nobukawa, Nishimura, et al. 2021a; Nobukawa, Wagatsuma, et al. 2021b). PV interneurons are the largest inhibitory population and mainly inhibit themselves and Pyr neurons. SOM interneurons transmit signals to all other neuronal populations. VIP interneurons suppress the responses of SOM neurons and are activated by feedback signals mediating selective attention. Simulations of our proposed model suggested that selective attention induces gamma activity modulations; this is in agreement with physiological reports from the monkey visual cortex (Womelsdorf et al. 2006; Bosman et al. 2012). Of note, simulations of our model implied that the activation of PV and SOM neurons contributes to the preferential generation of gamma and beta oscillations, respectively, in the cortical microcircuit. Again, this is in agreement with observed physiological results (Chen et al. 2017; Veit et al. 2017). Additionally, our model predicted that rapid and marked inhibitory transmission from VIP to SOM neurons is key for the attentional modulation of activity in layers 2/3 of the V1. These findings were obtained from simulations of the microcircuit model while various inputs and synaptic weights and delays were applied. Our results suggest that distinct subtypes of inhibitory interneurons have different roles in the regulation and modulation of neuronal activity for visual perception. Our microcircuit model also suggests the possible structure of a functional unit of layers 2/3 in the V1 for the integration of different neural signals and the establishment of visual perception.

Materials and methods

Architecture of the proposed model

Our microcircuit model consisted of excitatory Pyr neurons and 3 subtypes of inhibitory interneurons—PV, SOM, and VIP—with a biologically plausible cortical structure and network that mimicked layers 2/3 of the V1. The architecture of the proposed microcircuit model, which represented the fundamental unit of the visual cortex, is illustrated in Fig. 1(a). The arrows in Fig. 1(a) represent neuronal connections; the triangular and circular arrowheads indicate excitatory and inhibitory connections, respectively.

The total number of neurons and the connection probabilities in the proposed microcircuit were based on previous computational studies of the laminar structure of the visual cortex (Wagatsuma et al. 2011; Wagatsuma et al. 2013; Potjans and Diesmann 2014). The details of the parameters for the network are listed in Table 1. However, because of computational resource and cost limitations, we used a reduced number of model neurons compared with previous studies. The full network of our model, representing layers 2/3 in the V1, comprised around 2,650 integrate-and-fire neurons (2,068 Pyr, 268 PV, 175 SOM, and 140 VIP neurons) and around 900,000 synapses. The relative numbers of each neuron subtype were based on data derived from physiological experiments (Rudy et al. 2011; Pfeffer et al. 2013) and a computational model (Lee et al. 2017). For the detailed methods used to determine the population sizes for each neuron class and subtype, see Lee et al. (2017). The neuronal microcircuit that consisted of these local neuron populations represented a functional unit in the V1. For simplicity, we did not consider the spatial locations of these model neurons (Potjans and Diesmann 2014).

The connectivity from excitatory Pyr neurons to the 3 inhibitory interneuron subtypes was set to be similar to the superficial-layer structure of a previous network model (Lee et al. 2017). In this earlier model, the 3 inhibitory interneuron subtypes were equally connected to the Pyr neurons, which meant that the number of synaptic connections from Pyr neurons was determined by the size of the postsynaptic neuron subtype (Potjans and Diesmann 2014; Lee et al. 2017).

We thus connected the 3 inhibitory neuron subtypes to Pyr neurons using the methods of this previous model (Lee et al. 2017). We computed the total number of synapses from inhibitory interneurons to Pyr neurons; these were divided into 3 populations using the connection probabilities reported in Pfeffer et al. (2013) as weighting factors (Table 1). In our model, excitatory Pyr neurons mainly received inhibitory inputs from PV and SOM neurons. In the same way, we introduced recurrent connections among the 3 inhibitory neuron populations (Table 1). Figure 1a shows the cell-subtype-specific inhibitory connections of our model. This connectivity was adapted from earlier circuit diagrams that were based on physiological and computational studies (Pfeffer et al. 2013; Lee et al. 2017, 2018).

Physiological studies have reported that the distribution of excitatory postsynaptic potential (EPSP) amplitude between cortical Pyr neurons were well fitted to the log-normal distribution, which shaped the Gaussian distribution when plotted on a log scaled x-axis (Song et al. 2005; Lefort et al. 2009). In our model, the strengths of the synaptic conductance between excitatory Pyr neurons were distributed according to a long-tailed, log-normal distribution (Teramae et al. 2012; Nobukawa, Nishimura, et al. 2021a; Nobukawa, Wagatsuma, et al. 2021b). By contrast, the strengths of synaptic conductance for excitatory-to-inhibitory, inhibitory-to-excitatory, and

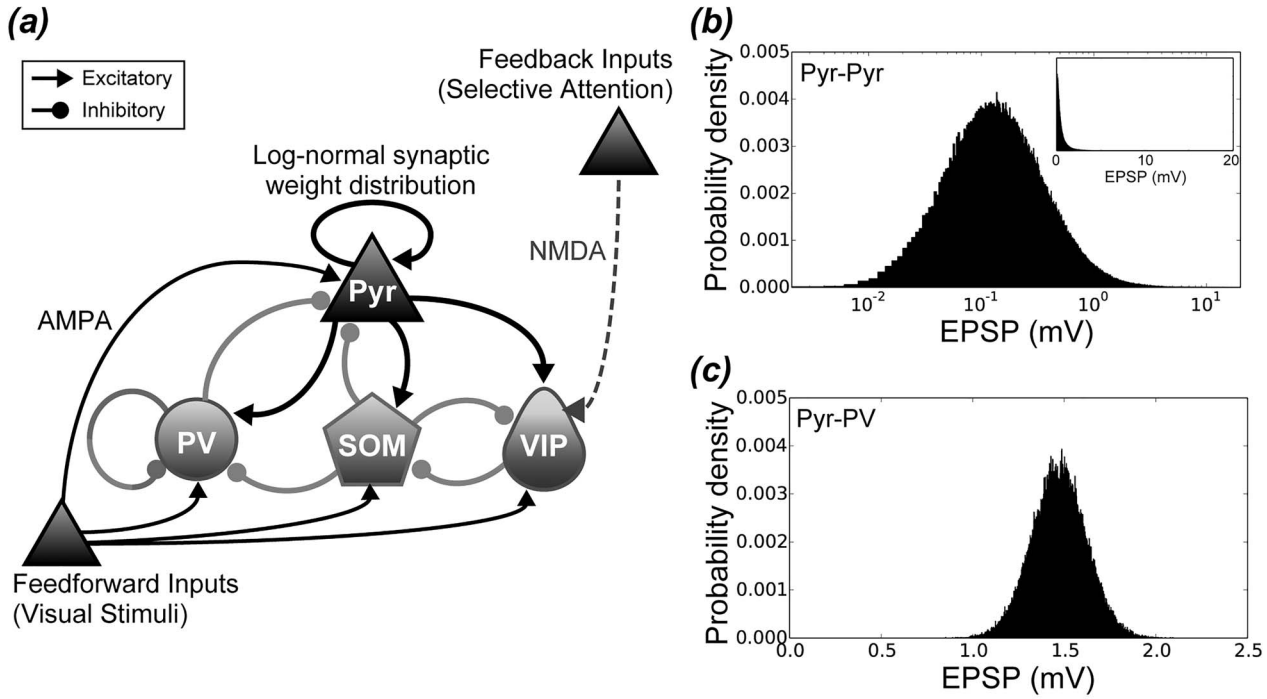

Fig. 1. Architecture of the proposed microcircuit model for cortical layers 2/3 of the V1. a) The microcircuit model consisted of excitatory Pyr neurons and 3 subtypes (PV, SOM, and VIP) of inhibitory interneurons. The triangle, circle, pentagon, and teardrop shapes represent the Pyr, PV, SOM, and VIP neuronal populations, respectively. The neurons used in the construction of the microcircuit are pictured as integrate-and-fire neurons. Arrows with triangular and circular heads represent excitatory and inhibitory synaptic connections, respectively. Excitatory synaptic connections within this cortical microcircuit network and feedforward inputs (visual stimuli) are driven by AMPA receptors, whereas feedback signals (selective attention) rely on NMDA receptors (Wagatsuma et al. 2016, 2021). Excitatory synaptic weights between Pyr neurons were distributed according to a log-normal distribution (Song et al. 2005; Lefort et al. 2009; Teramae et al. 2012). By contrast, the synaptic weights for excitatory-to-inhibitory, inhibitory-to-excitatory, and inhibitory-to-inhibitory connections obeyed a Gaussian distribution. Details of the distributions of synaptic weights are shown in panels (b) and (c). b) Distribution of synaptic weights between excitatory Pyr neurons. Each excitatory Pyr neuron had a log-normal amplitude distribution of EPSPs. Note that the x-axis of the main plot is on a log scale. The inset graph is a normal plot of the same distribution. c) Example distribution of synaptic weights for excitatory-to-inhibitory neurons (from Pyr to PV neurons). In our model, the synaptic weights for excitatory-to-inhibitory, inhibitory-to-excitatory, and inhibitory-to-inhibitory connections obeyed Gaussian distributions.

Table 1. Parameters for the network architecture of our microcircuit model.

The number of neurons			
Pyr	**PV**	**SOM**	**VIP**
2068	268	175	140
Connection probabilities between neuron classes			
Excitatory-to-Excitatory	**Excitatory-to-Inhibitory**	**Inhibitory-to-Excitatory**	**Inhibitory-to-Inhibitory**
0.1009	0.1346	0.1689	0.1371
Weighting factors for neuron-subtype-specific connections			
Inhibitory-to-Excitatory		**Inhibitory-to-Inhibitory**	
PV-Pyr:SOM-Pyr = 1:1		PV-PV:SOM-PV:VIP-SOM:SOM-VIP = 1:0.857:0.625:1	

The connection probabilities and weighting factors were based on Potjans et al. (2014) and Lee et al. (2017), respectively.

inhibitory-to-inhibitory synapses obeyed Gaussian distributions. We describe the details of these synaptic parameters in the following subsections.

Our microcircuit model involved 3 types of external inputs: background inputs, to induce spontaneous activity; feedforward inputs, representing bottom-up visual stimuli; and modulatory feedback signals, mediating selective attention. From physiological studies, feedforward inputs are mediated by glutamatergic α-amino-3-hydroxy-5-methyl-4-isoxazolepropionic acid (AMPA) receptors, whereas modulatory feedback signals take the form of currents through N-methyl-D-aspartate (NMDA) receptors (Self et al. 2012; Herrero et al. 2013). The detailed mathematical descriptions of these inputs as applied in the model are provided in the "Model neurons and synapses" section.

Model neurons and synapses

In the present study, all classes and subtypes of model neurons were described by integrate-and-fire neurons (Buehlmann and Deco 2008; Wagatsuma et al. 2016, 2021). The dynamics of the subthreshold membrane potential (V) of a model neuron were described by the following:

$$\frac{dV(t)}{dt} = -\frac{V(t) - E_l}{\tau_m} + \frac{I_{\mathrm{Pyr}}(t) + I_{\mathrm{PV}}(t) + I_{\mathrm{SOM}}(t) + I_{\mathrm{VIP}}(t) + I_{\mathrm{ext}}(t)}{C_m}, \quad (1)$$

Table 2. Neuronal model parameters for each class of neurons.

		Parameter			
		Pyr	PV	SOM	VIP
τ_m	Membrane time constant (ms)	10.5	3.1	11.8	10.9
τ_{ref}	Refractory period (ms)		2.0		
C_m	Membrane capacitance (pF)		200		
E_l	Leak reversal potential (mV)		−70		

where τ_m is the membrane time constant and C_m is the membrane capacitance. E_l represents the leak-reversal potential. The neuronal model parameters are summarized in Table 2 and were chosen based on previous studies (Buehlmann and Deco 2008; Neske et al. 2015; Lee et al. 2018). The spike threshold was $V_{thr} = -50$ mV and the membrane potential V reset to $V_{reset} = -60$ mV after spiking. The $I_{Pyr}(t)$, $I_{PV}(t)$, $I_{SOM}(t)$, and $I_{VIP}(t)$ represent the synaptic currents that flowed into the model neuron from the Pyr, PV, SOM, and VIP neuron classes, respectively.

The $I_{Pyr}(t)$, which represented synaptic currents from excitatory Pyr neurons as mediated by AMPA-type currents (Buehlmann and Deco 2008; Deco and Thiele 2011), was defined as

$$I_{Pyr}(t) = g_j^{Pyr}\,(V(t) - V_E)\sum_j s_j^{Pyr}(t), \tag{2}$$

where $V_E = 0$ mV represents the reversal potential of the excitatory Pyr neurons, and V is the subthreshold membrane potential of a model neuron (see also Eq. (1)). The conductance of the fully activated synapse g^{Pyr} is the receptor-specific conductance. The distribution of the strengths of g^{Pyr} values between Pyr neurons was distinct from the distributions of the other connection types (Teramae et al. 2012). This is described further in the "Distributions of strengths and delays of postsynaptic currents" section. The fraction of open channels of model neurons from the jth Pyr neuron (s_j^{Pyr}) was determined as follows:

$$\frac{ds_j^{Pyr}}{dt} = -\frac{s_j^{Pyr}(t)}{\tau_{Pyr}} + \sum_k \delta\left(t - t_j^k - d_j\right), \tag{3}$$

where the postsynaptic-decay time constant is $\tau_{Pyr} = 2.0$ ms irrespective of the class of postsynaptic neuron. The sum over k runs over all spikes from connecting Pyr neurons. Each spike was entered as a Dirac delta function, $\delta(t)$, assuming a non-0 value at the spike times of the visually driven input neurons (t_j^k) (0 elsewhere) and integrating to unity over any interval that included t_j^k. The d_j is the delay from the jth Pyr neuron.

Synaptic currents from the 3 subtypes of inhibitory interneurons reduced the membrane potentials of postsynaptic model neurons. Synaptic currents from inhibitory model interneurons I_{Inh} were defined as follows:

$$I_{Inh}(t) = g_j^{Inh}\,(V(t) - V_I)\sum_j s_j^{Inh}(t), \tag{4}$$

where the subscript Inh of I_{Inh} represents the subtype of inhibitory neuron: PV, SOM, or VIP; $V_I = -70$ mV is the reversal potential of the inhibitory interneurons; g^{Inh}, which represents the synaptic conductance of a fully open synapse of a specific subtype of inhibitory interneuron, was determined by the connections between neuron classes (Table 3; Lee et al. 2018; Hoffmann et al. 2015). The fraction of open channels in a PV, SOM, or VIP synapse is s_j^{Inh}, which was determined as follows:

$$\frac{ds_j^{Inh}}{dt} = -\frac{s_j^{Inh}(t)}{\tau_{Inh}} + \sum_k \delta\left(t - t_j^k - d_j\right), \tag{5}$$

where τ_{Inh} is the postsynaptic decay time constant; this was selected based on previous studies (Table 3; Pfeffer et al. 2013; Lee et al. 2018). As in the description of synaptic currents for Pyr neurons in Eq. (3), the sum over k is over spike time (t_j^k); here, these were the times of spikes occurring in the inhibitory interneurons.

Recent studies have provided estimates of neuron-subtype-specific postsynaptic currents, such as synaptic conductance (g^{Pyr} and g^{Inh}) and decay time constants (τ_{Pyr} and τ_{Inh}) (Pfeffer et al. 2013; Hoffmann et al. 2015; Lee et al. 2017, 2018). Table 3 summarizes the details of the synaptic parameters used to construct our model. Because of the larger scale of the model network compared with that of Lee et al. (2018), we slightly decreased the magnitude of peak currents in our microcircuit model. Furthermore, in our model, we introduced marked excitatory connections from Pyr neurons to VIP interneurons (Lee et al. 2017); this strongly inhibited the activity of SOM interneurons. To compensate for this inhibition, we decreased the magnitude of peak currents from VIP to SOM interneurons. On the basis of previous studies (Wagatsuma et al. 2011, 2013; Potjans and Diesmann 2014; Lee et al. 2017), the connectivity between 2 model neurons was determined by the neuron classes and not their spatial location.

The $I_{ext}(t)$ in Eq. (1) represents the synaptic currents of external inputs to model neurons. In our network model, all model neuron populations received background inputs and feedforward inputs, which were mediated by AMPA-type synapses. Feedforward inputs originate with visual stimuli. Modulatory feedback signals represent selective attention and are mediated by NMDA-type synapses (Self et al. 2012; Herrero et al. 2013; Wagatsuma et al. 2016, 2021). Feedback signals were applied to VIP neurons (Buia and Tiesinga 2008; Pi et al. 2013; Pfeffer 2014; Zhang et al. 2014; Lee et al. 2018; Wilmes and Clopath 2019), which modulated interactions between VIP and SOM neurons. In our model, attentional modulation of Pyr neurons occurred via the interactions between VIP and SOM inhibitory interneurons (Buia and Tiesinga 2008; Lee et al. 2018). The parameters and connection probabilities for these external inputs are given in Table 4.

All neurons in our model received cell-subtype-specific background inputs, which induced and preserved spontaneous activity without sensory inputs. Background inputs to each model neuron were given using an independent Poisson spike train. Feedforward inputs, which were also described by independent Poisson spike trains, projected to their target model neuron populations; these were randomly chosen according to connection probabilities (see Table 4). We set the population size for these feedforward inputs

Table 3. Parameters of neuron-class-specific postsynaptic currents for synaptic conductance and decay time constants.

	From			
To	Pyr	PV	SOM	VIP
Synaptic conductance g (nS), mean ± SD				
Pyr	See main text	3.36 ± 0.336	1.96 ± 0.196	–
PV	1.47 ± 0.147	5.46 ± 0.546	1.89 ± 0.189	–
SOM	0.45 ± 0.045	–	–	0.50 ± 0.050
VIP	0.41 ± 0.041	–	1.84 ± 0.184	–
Synaptic-decay time constants τ_d (ms)				
Pyr	2.0	6.4	13.1	–
PV	2.0	4.6	5.2	–
SOM	2.0	–	–	13.1
VIP	2.0	–	10.2	–

at 100 fibers. Such background and feedforward inputs are mediated by glutamatergic AMPA receptors (Buehlmann and Deco 2008; Deco and Thiele 2011) and were defined as

$$I_{\mathrm{Input}}(t) = g_j^{\mathrm{Input}}\left(V(t) - V_E\right)\sum_j s_j^{\mathrm{Input}}(t), \tag{6}$$

where g^{Input} is the conductance of the fully activated synapse for the background or feedforward input. The fraction of open channels of model neurons from the jth Poisson spike train (s_j^{Input}) was determined as

$$\frac{ds_j^{\mathrm{Input}}}{dt} = -\frac{s_j^{\mathrm{Input}}(t)}{\tau_{\mathrm{Input}}} + \sum_k \delta\left(t - t_j^k - d_j\right), \tag{7}$$

where the postsynaptic decay time constant for the background and feedforward inputs is $\tau_{\mathrm{Input}} = 2.0$ ms irrespective of the class of target neuron. See also Eqs (3) and (5) for the detailed descriptions of these equations.

In the current study, VIP interneurons received modulatory feedback signals that mediated selective attention (Fig. 1(a)). The feedback signals were sets of Poisson spike trains at 20 Hz. We set the population size for these signals to 100 fibers, and the projection probabilities of the feedback connections were within a physiologically realistic range. These modulatory feedback signals rely on NMDA-type projections (Self et al. 2012; Herrero et al. 2013). All NMDA receptors have a voltage dependence that is controlled by $[Mg^{2+}]$ (Jahr and Stevens 1990), which we assumed to be $[Mg^{2+}] = 1$ mM. Here, we used a standard computational model for generic NMDA receptors (Wang 1999) in which the NMDA-receptor-mediating synaptic current, I_{fb}, was defined as follows:

$$I_{\mathrm{fb}}(t) = \frac{g_j^{\mathrm{NMDA}}\left(V(t) - V_E\right)}{1 + \left[Mg^{2+}\right]\exp\left(-0.062V(t)\right)/3.57}\sum_j s_j^{\mathrm{NMDA}}(t), \tag{8}$$

where g^{NMDA} is the synaptic conductance of a fully open NMDA synapse. The fraction of open NMDA channels in a synapse is s_j^{NMDA}, which was calculated as

$$\frac{ds_j^{\mathrm{NMDA}}(t)}{dt} = -\frac{s_j^{\mathrm{NMDA}}(t)}{\tau_{\mathrm{NMDA,decay}}} + \alpha x(t)\left(1 - s_j^{\mathrm{NMDA}}(t)\right), \tag{9}$$

$$\frac{dx(t)}{dt} = -\frac{x(t)}{\tau_{\mathrm{NMDA,rise}}} + \sum_k \delta\left(t - t_{\mathrm{fb}}^k\right), \tag{10}$$

where $\alpha = 1$/ms. The rise time for an NMDA synapse is $\tau_{\mathrm{NMDA,rise}} = 2$ ms, and their decay time constant is $\tau_{\mathrm{NMDA,decay}} = 100$ ms (Buehlmann and Deco 2008). As in the description of AMPA synaptic currents in Eqs (3), (5), and (7), the sum over k is over spike time (t_{fb}^k); here, it is the times at which spikes occur in the Poisson spike train, representing feedback signals.

Distributions of strengths and delays of postsynaptic currents

The synaptic parameter values for synaptic conductance g and decay time constant τ_{decay} in our network model were estimated and selected based on previous studies (Table 3; Pfeffer et al. 2013; Lee et al. 2017, 2018). In our model, the strengths of synaptic conductance g for excitatory-to-inhibitory, inhibitory-to-excitatory, and inhibitory-to-inhibitory synapses obeyed a Gaussian distribution. By contrast, the strengths of conductance between excitatory Pyr neurons were distributed according to a log-normal distribution (Song et al. 2005; Lefort et al. 2009; Teramae et al. 2012; Nobukawa, Nishimura, et al. 2021a; Nobukawa, Wagatsuma, et al. 2021b), as follows:

$$p(x) = \frac{\exp\left[-\left(\log x - \mu\right)^2/2\sigma^2\right]}{\sqrt{2\pi}\sigma x}, \tag{11}$$

where x represents the amplitude of EPSPs measured from the resting potential; σ and μ represent the mean and variance, respectively. In the present study, we used $\sigma = 1.0$ and $\mu - \sigma^2 = \log(0.125)$ to represent biologically plausible spontaneous activity under the application of background inputs. For simplicity, we used a standard computational model and decay time constant $\tau_{\mathrm{Pyr}} = 2.0$ ms for generic AMPA receptors as synapses between Pyr neurons (see also Eqs. (2) and (3)).

Synaptic delays are important factors for determining the activity and dynamics of neuronal networks (Teramae et al. 2012). In the current study, synaptic delays were distributed according to Gaussian distribution, with mean d_0 and variance $d_0/10$; $d_0 = 2.0$ ms for connections from excitatory Pyr neurons and $d_0 = 1.0$ ms for connections from the 3 inhibitory interneuron subtypes. For simplicity, the values of synaptic delays were independent of the inhibitory neuron subtype. Similar to the synaptic weights, these delays were not determined by the spatial locations of model neurons.

Table 4. Parameters of external excitatory inputs.

Background inputs to each neuron class mediated by AMPA synaptic currents					
		Parameter			
		Pyr	**PV**	**SOM**	**VIP**
g^{BG}	Conductance (nS)	10.0	10.0	10.0	10.0
τ_d	Decay time constant (ms)	2.0	2.0	2.0	2.0
ν_{BG}	Rates (Hz)	190	770	140	200
Feedforward inputs to each class of neuron population mediated by AMPA synaptic currents					
		Parameter			
		Pyr	**PV**	**SOM**	**VIP**
# of fibers		100	100	100	100
Connection probability		0.1	0.01	0.01	0.01
g^{FF}	Conductance (nS)	6.0	6.0	6.0	6.0
τ_d	Decay time constant (ms)	2.0	2.0	2.0	2.0
ν_{FF}	Rates (Hz)	25	25	25	25
Feedback signals to the VIP neuron population mediated by NMDA synaptic currents					
		Parameter			
		VIP			
# of fibers		100			
Connection probability		0.075			
g^{FB}	Conductance (nS)	4.0			
$\tau_{NMDA,decay}$	Decay time constant (ms)	100.0			
$\tau_{NMDA,rise}$	Rise time constant (ms)	2.0			
ν_{FB}	Rates (Hz)	20			

Numerical experiments

In the current study, we performed numeric simulations using our model under various conditions. During the simulations, background inputs were applied to all model neurons to induce spontaneous responses. Additionally, we applied feedforward inputs, representing visual stimuli, and modulatory feedback signals, mediating selective attention, to the network model. Note that both the background and feedforward inputs were simultaneously provided to the network during the simulations with visual stimuli (the visual stimulus condition). Many previous studies have reported attentional modulation with respect to neuronal activity and synchronized oscillations during sensory processing (Womelsdorf et al. 2006; Bosman et al. 2012; Zhang et al. 2014; Bastos et al. 2015; Richter et al. 2017; Rohenkohl et al. 2018). In our model, to investigate the mechanism of modulation by feedback signals and to simulate the model with selective attention (the attention condition), we applied feedback signals to VIP interneurons (Buia and Tiesinga 2008; Pi et al. 2013; Pfeffer 2014; Zhang et al. 2014; Lee et al. 2018; Wilmes and Clopath 2019). To simulate the attention condition, our microcircuit model integrated background and feedforward inputs with feedback signals.

We integrated the differential equations using a fourth-order Runge–Kutta algorithm with a time step of 0.1 ms. We simulated 50 trials with a length of 6 biological s per condition to ensure the reproducibility of model responses. The first 1 s of simulated results was always discarded to minimize the effects of transients. The code for the simulations was written in C programming language.

Data analysis of responses in the proposed network model

To investigate the roles of specific inhibitory interneuron subtypes in the regulation and modulation of neuronal responses and synchronizations of layers 2/3 in the V1, we analyzed the population rates of all classes of model neurons as the representative activity of the network model. The mean population rates were computed by counting the total number of spikes in each class of neuron between 1 and 6 biological s and by averaging this number over 50 trials.

For a more detailed investigation of the contribution of activity in specific subtypes of inhibitory interneurons to the modulation of cortical responses in the V1, we used spike-time histograms (STHs) of the Pyr neuron population between 1 and 6 s of simulation data. In previous computational studies, the STHs of excitatory model neurons were used to model local field potentials (LFPs) (Buia and Tiesinga 2008; Lee et al. 2018). A linear combination of excitatory and inhibitory synaptic currents arising from a spiking neuron network might be more suitable for modeling LFPs (Mazzoni et al. 2015). However, we analyzed STHs to reduce computational costs.

The STH represents an estimate of the time-varying firing rates of a population. It was obtained by dividing the firing activity of Pyr neurons into discrete time bins of 2 ms and counting the number of spikes that fell in each time bin. We analyzed the frequency characteristics of these model STHs with respect to various simulation conditions. The STHs of Pyr neurons were decomposed into frequency components using the fast Fourier

transform, and the mean oscillation amplitude was computed by averaging the amplitudes of the STHs. These data analyses and visualizations were performed using Python programming language.

Results

We developed a biologically plausible network model to understand the microcircuit structure of layers 2/3 in the V1 and to investigate the roles of inhibitory interneurons in the regulation of neuronal responses. The architecture of our model, with Pyr neurons and 3 subtypes of interneurons, is illustrated in Fig. 1(a). We performed simulations of the model under various conditions to investigate the roles of specific subtypes of inhibitory interneurons in the regulation of neuronal responses and in the synchronization of layers 2/3 in the V1.

Responses of the proposed microcircuit model to visual stimuli and selective attention

First, we investigated the influence of feedforward inputs (representing visual stimuli) and feedback signals (mediating selective attention) in modulating the responses of the microcircuit of layers 2/3 in the V1. During the simulations, all model neurons received cell-class-specific background inputs to induce spontaneous responses. For the visual stimulus condition, feedforward inputs originating from visual stimuli were added to all neuron classes. In the selective attention condition, we also applied modulatory feedback signals—representing selective attention—to VIP interneurons. Figure 2a shows spike raster plots of all neuron classes and subtypes over 2 biological s. In this simulation, visual stimuli were presented from 500 biological ms and selective attention was activated from 1 s. The activity of all neuron classes and subtypes was markedly modulated by both visual stimuli and selective attention.

Figure 2b shows the mean population rates of all neuron classes and subtypes in the spontaneous, visual stimulus, and selective attention conditions. In the spontaneous condition, the population rates of each neuron class fell within a physiologically realistic range (Pyr ∼0.6 Hz, PV ∼6.2 Hz, SOM ∼2.8 Hz, and VIP ∼5.2 Hz). The application of visual stimuli substantially modulated activity in all neuron classes. The Pyr neurons and PV and SOM interneurons were activated by visual stimuli, whereas the projections of visual stimuli to our microcircuit inhibited VIP interneuron responses. Furthermore, the feedback signals (mediating selective attention) markedly increased VIP interneuron activity and decreased SOM interneuron activity. The Pyr neurons and PV interneurons were also activated by the application of selective attention to the microcircuit, perhaps because of the attention-induced inhibition of SOM interneurons. This modulation pattern of Pyr neuron activity by these external inputs is consistent with the physiological patterns observed in V1 neurons (McAdams and Maunsell 1999; Martinez-Trujillo and Treue 2004). Of interest, in our model, the modulation patterns of SOM interneurons in response to feedforward inputs and feedback signals were the opposite of those of VIP interneurons.

Visual stimuli and selective attention not only activated Pyr neurons but also seemed to induce and modulate the synchronized oscillatory responses of this neuron class (Fig. 2(a)). To investigate the mechanism underlying the integration of various inputs in the cortical microcircuit, the STHs of Pyr neurons were computed based on time bins of 2 ms and were decomposed into frequency components using the fast Fourier transform (see Materials and methods). Figure 2(c) summarizes the STH power of Pyr neurons averaged over 50 simulation trials in the spontaneous, visual stimulus, and selective attention conditions. There was no clear peak in the STH power of Pyr neurons in the spontaneous condition (dashed line). By contrast, application of visual stimuli to our microcircuit model induced peak beta-band activity between 20 and 30 Hz (black line). Low (30–50 Hz) and high (50–100 Hz) gamma-band activity increased from the visual stimulus condition (black line) to the selective attention condition (gray line). Intriguingly, under the selective attention condition, there were 2 peaks in the range of low-gamma (around 35 Hz) and high-gamma (around 65 Hz) activity. These results imply that feedforward inputs (representing visual stimuli) generate oscillatory responses of beta-band activity in the microcircuit of layers 2/3 in the V1, whereas feedback signals (mediating selective attention) modulate gamma activity. This attentional modulation of gamma activity is in agreement with physiological reports of the monkey visual cortex (Womelsdorf et al. 2006; Bosman et al. 2012). Selective attention enhanced gamma-band activity and increased activity in Pyr neurons and PV interneurons and decreased SOM interneuron responses (Fig. 2(b)). These results suggest that PV interneurons contribute to the preferential generation of gamma oscillation in cortical layers 2/3 of the V1.

Cell-subtype-specific synaptic strengths for the modulation of responses and synchronized oscillation in the microcircuit

Many studies have reported the key contributions of the distinct inhibitory interneuron subtypes to the generation of specific bands of synchronized oscillation (Chen et al. 2017; Cardin 2018; Lee et al. 2018). To obtain a mechanistic insight into the functions of the distinct interneuron subtypes in the modulation of responses and the synchronized oscillation in the V1, we performed simulations of the model with various synaptic strengths for the different connections in our network. During these simulations, we applied feedforward inputs (visual stimuli) to our model. The simulation results of our model with various synaptic strengths are summarized in Fig. 3.

We first performed simulations of our microcircuit model with various synaptic strengths from Pyr neurons to PV interneurons ($W_{Pyr\text{-}PV}$). Spike raster plots of Pyr neurons with various $W_{Pyr\text{-}PV}$ are shown in Fig. 3(a). Regardless of $W_{Pyr\text{-}PV}$, the response of Pyr neurons to visual stimuli was rhythmically activated. However, both the density and rhythm of the synchronized responses of Pyr neurons seemed to be modulated by $W_{Pyr\text{-}PV}$. The population rates of all neuron classes are presented in Fig. 3(b) as functions of $W_{Pyr\text{-}PV}$. Both Pyr neurons and SOM interneurons were increasingly activated as $W_{Pyr\text{-}PV}$ decreased, whereas the rates of the other populations decreased with decreasing $W_{Pyr\text{-}PV}$. Decreasing $W_{Pyr\text{-}PV}$ not only inhibited PV interneuron activity but also activated interactions between Pyr neurons and SOM interneurons. To analyze the influence of $W_{Pyr\text{-}PV}$ on the modulation of responses in cortical layers 2/3, we computed the STH power of Pyr neurons with respect to various $W_{Pyr\text{-}PV}$ (Fig. 3(c)). The magnitude of beta-band activity for the range between 20 and 30 Hz was markedly increased with decreasing $W_{Pyr\text{-}PV}$ (red line); this seemed to arise from the facilitation of interactions between Pyr neurons and SOM interneurons. In this condition, SOM interneurons and Pyr neurons were activated, whereas PV interneurons were inhibited (Fig. 3(b)). Activated SOM interneurons might have more influence on the responses of Pyr neurons than on those of inhibited PV interneurons. Conversely, increasing $W_{Pyr\text{-}PV}$ markedly decreased the power of beta-band activity (green and blue lines). These results suggest a role for interactions between Pyr neurons and

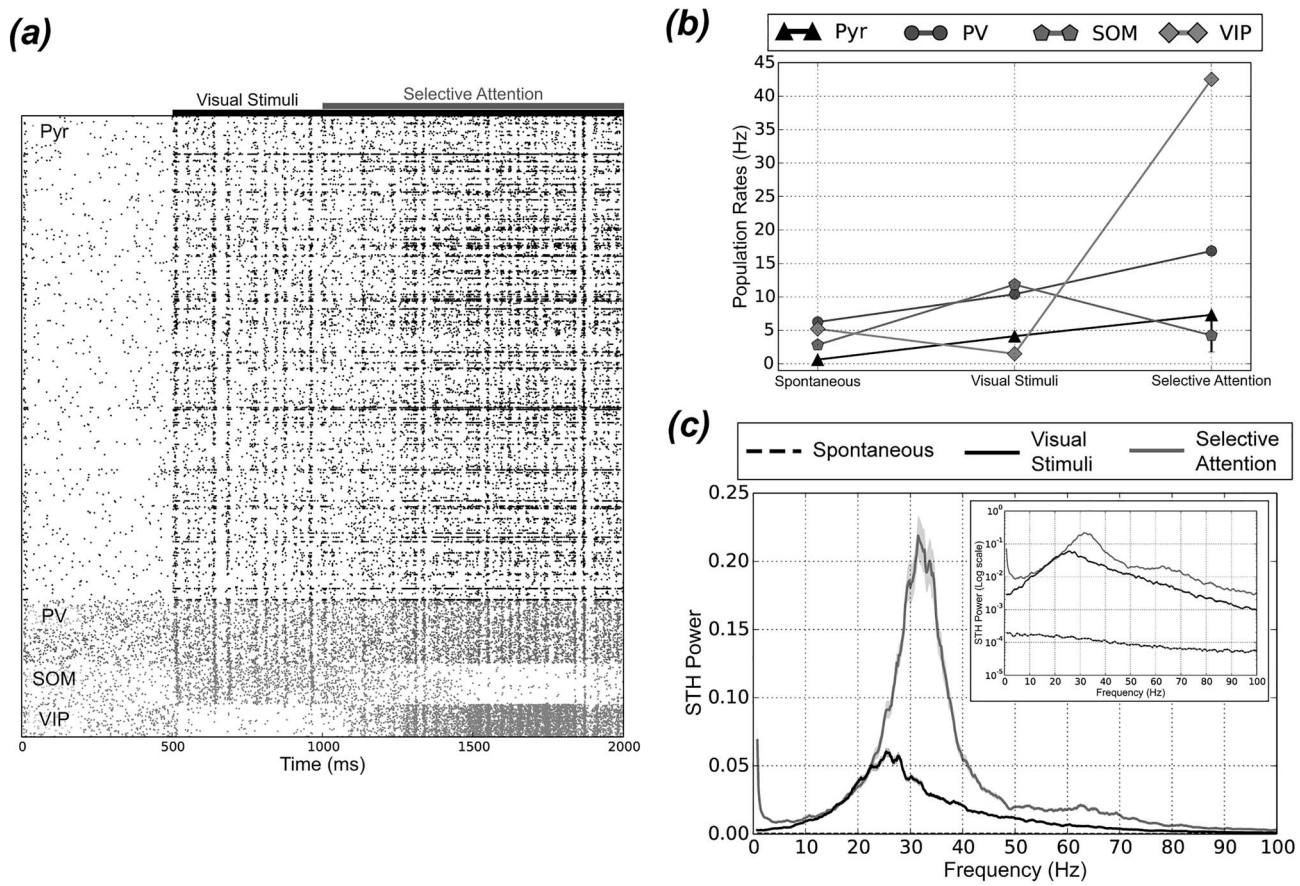

Fig. 2. Neuronal responses in the proposed microcircuit model. a) Raster plots showing spike trains of Pyr, PV, SOM, and VIP neurons for 2 s. The spikes of excitatory Pyr neurons and the three inhibitory interneuron subtypes are illustrated with black and gray dots, respectively. For this plot, visual stimuli were presented during the period represented by the black bar at the top of the panel (500 ms–2 s) and selective attention was activated during the period represented by the gray bar (1–2 s). The activity of neurons in our microcircuit model was modulated by these 2 external inputs. b) The mean population firing rates of Pyr (triangles), PV (circles), SOM (pentagons), and VIP (squares) neurons in the microcircuit model, taken from 50 simulation trials of the spontaneous, visual stimulus, and selective attention conditions. Error bars indicate the standard errors (SEs), which were relatively small in these simulations. c) STH power of Pyr neurons, averaged over 50 simulation trials in the spontaneous (black dashed line), visual stimulus (black solid line), and selective attention (gray solid line) conditions. The inset shows a log-scale plot of the same STH power results. The shading of the curves indicates the SE of the mean from 50 simulation trials.

SOM interneurons in the generation of visually induced beta oscillation. Additionally, the power of low-gamma-band (30–50 Hz) activity slightly increased (decreased) with increases (decreases) in SOM interneuron firing rates. These simulation results for the contributions of SOM interneuron spiking to the generation of neuronal oscillations around 30 Hz are in agreement with the results of physiological studies (Roopun et al. 2010; Chen et al. 2017; Veit et al. 2017). Furthermore, with increased $W_{Pyr\text{-}PV}$, the peak of STH power shifted toward the range of low-gamma-band activity rather than beta-band activity (green and blue lines in Fig. 3(c)) in addition to the activation of PV interneurons (Fig. 3(b)).

To further investigate the contributions of the 3 inhibitory interneuron subtypes, we tested our model with various synaptic strengths from Pyr neurons to SOM interneurons ($W_{Pyr\text{-}SOM}$). Figure 3(d) shows spike raster plots of Pyr neurons with various $W_{Pyr\text{-}SOM}$. Decreased $W_{Pyr\text{-}SOM}$ seemed not only to activate Pyr neurons but also to narrow the window for synchronized spiking in this population. The population rates of all neuron classes except SOM interneurons increased with decreasing $W_{Pyr\text{-}SOM}$ (Fig. 3(e)). In the responses of our microcircuit model with $0.25 \times W_{Pyr\text{-}SOM}$, SOM interneuron activity was markedly lower than that of other neuron classes. Therefore, under this condition, Pyr neuron responses seemed to be determined by interactions with PV interneurons. Additionally, the magnitude of gamma-band activity between 30 and 100 Hz increased as $W_{Pyr\text{-}SOM}$ decreased (red and purple lines in Fig. 3(f)), which might have been the result of the coactivation of Pyr neurons and PV interneurons and the inhibition of SOM interneurons. These results imply that interactions between Pyr neurons and PV interneurons contribute to gamma oscillation generation in cortical layers 2/3 of the V1; these findings are consistent with physiological reports (Chen et al. 2017).

Simulations of our model with various synaptic strengths from SOM to PV interneurons suggest the contribution of interactions between Pyr neurons and SOM interneurons to the generation of visually induced beta (20–30 Hz) oscillations. In addition to the activation of the oscillatory responses of beta-band activity, there was coactivation of Pyr neurons and SOM interneurons, whereas PV interneuron activity was suppressed. In our microcircuit model, SOM interneurons had synaptic connections with other interneuron subtypes to regulate responses (Fig. 1(a)). We investigated the influence of synaptic strength from SOM to PV interneurons ($W_{SOM\text{-}PV}$) in the regulation of responses in the cortical microcircuit. Spike raster plots of Pyr neurons with various $W_{SOM\text{-}PV}$ are shown in Fig. 3(g). Increased $W_{SOM\text{-}PV}$ seemed to broaden the spiking window of Pyr neurons. The population

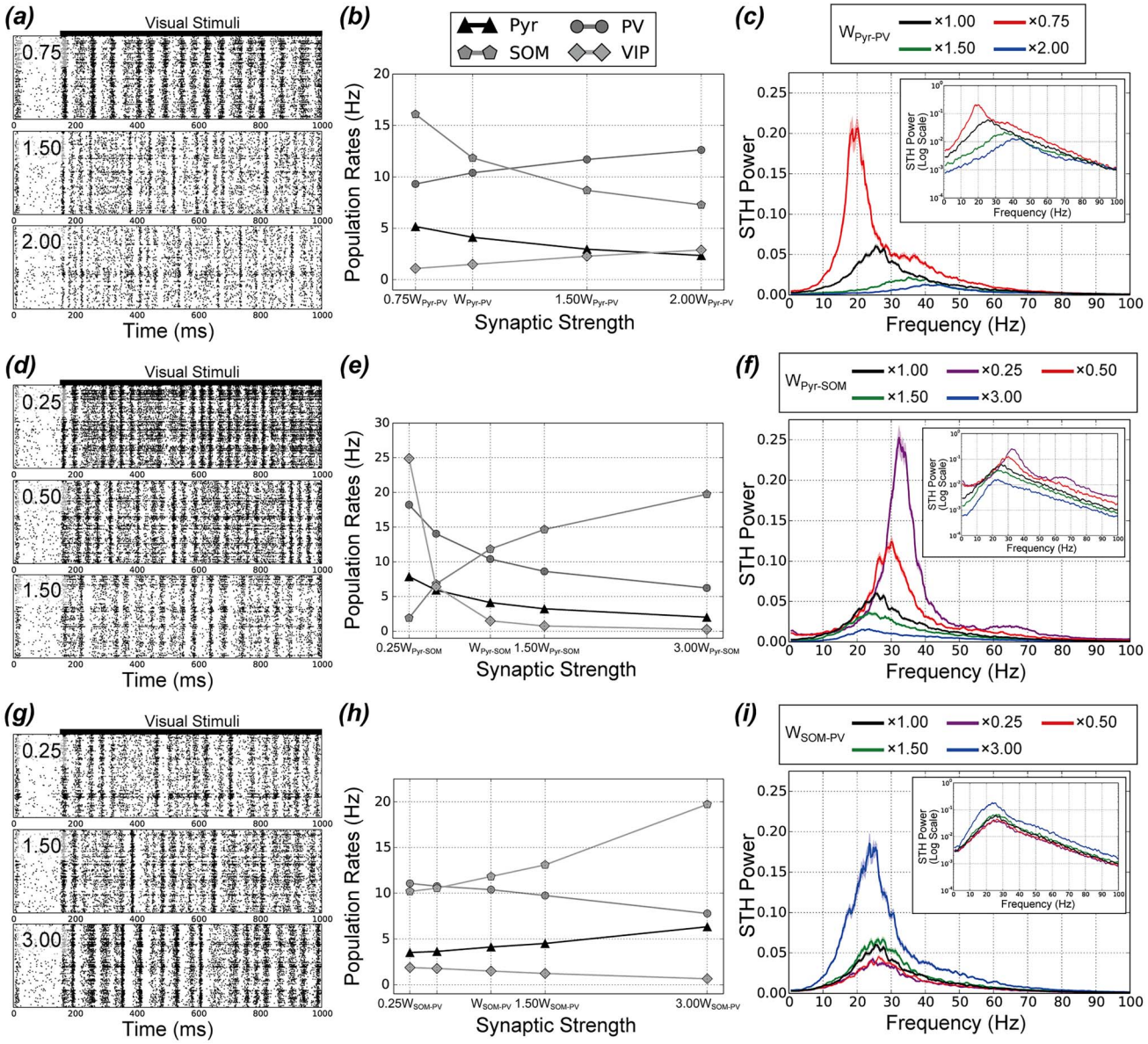

Fig. 3. Influence of synaptic strength on response modulation in the proposed microcircuit model. Panels (a–c), (d–f), and (g–h) demonstrate the model responses with various synaptic strengths from Pyr to PV ($W_{Pyr\text{-}PV}$), Pyr to SOM ($W_{Pyr\text{-}SOM}$), and SOM to PV ($W_{SOM\text{-}PV}$), respectively. In these simulations, we applied both background and visual stimuli to the model. The error bars in panels (b), (e), and (h) indicate SEs, which were relatively small in these simulations. The shading of the curves in panels (c), (f), and (i) indicate the SEs of the means from 50 simulation trials. a) Raster plots showing the spike trains of Pyr neurons for various $W_{Pyr\text{-}PV}$. The top, middle, and bottom panels represent the simulation results with 0.75, 1.50, and 2.00 × $W_{Pyr\text{-}PV}$, respectively. For these plots, visual stimuli were presented during the period indicated by the black bar at the top of the panel (150 ms–1 s). b) Mean population firing rates of Pyr (triangles), PV (circles), SOM (pentagons), and VIP (squares) neurons as functions of the strength of $W_{Pyr\text{-}PV}$ (based on 50 simulation trials). c) STH power of Pyr neurons averaged over 50 simulation trials versus $W_{Pyr\text{-}PV}$ (black line), 0.75 × $W_{Pyr\text{-}PV}$ (red line), 1.50 × $W_{Pyr\text{-}PV}$ (green line), and 2.00 × $W_{Pyr\text{-}PV}$ (blue line). The inset shows a log-scale plot of the same STH power results of the Pyr neurons. d) Raster plots showing all spike trains of the Pyr neurons in the model with respect to various $W_{Pyr\text{-}SOM}$. The top, middle, and bottom panels represent the Pyr neuron responses for 0.25 × $W_{Pyr\text{-}SOM}$, 0.50 × $W_{Pyr\text{-}SOM}$, and 1.50 × $W_{Pyr\text{-}SOM}$, respectively. e) Mean population firing rates of each neuron class for the different $W_{Pyr\text{-}SOM}$. In these simulations, $W_{Pyr\text{-}SOM}$ was set to 0.25, 0.50, 1.50, and 3.00 times that of our original model. All conventions are the same as those in panel (b). f) STH power of Pyr neurons averaged over 50 simulations for $W_{Pyr\text{-}SOM}$ (black line), 0.25 × $W_{Pyr\text{-}SOM}$ (purple line), 0.50 × $W_{Pyr\text{-}SOM}$ (red line), 1.50 × $W_{Pyr\text{-}SOM}$ (green line), and 3.00 × $W_{Pyr\text{-}SOM}$ (blue line). g) Raster plots of the Pyr neurons in the model with various $W_{SOM\text{-}PV}$. The top, middle, and bottom panels represent Pyr neuron activity with 0.25 × $W_{SOM\text{-}PV}$, 0.50 × $W_{SOM\text{-}PV}$, 1.50 × $W_{SOM\text{-}PV}$, and 3.00 × $W_{SOM\text{-}PV}$, respectively. h) Mean population firing rates of the neuron classes as functions of $W_{SOM\text{-}PV}$. All conventions are the same as those in panels (b) and (e). i) STH power of the Pyr neuron population averaged over 50 simulation trials for various $W_{SOM\text{-}PV}$. These curves were obtained using simulations with 1.00 × $W_{SOM\text{-}PV}$ (black line), 0.25 × $W_{SOM\text{-}PV}$ (purple line), 0.50 × $W_{SOM\text{-}PV}$ (red line), 1.50 × $W_{SOM\text{-}PV}$ (green line), and 3.00 × $W_{SOM\text{-}PV}$ (blue line).

rates of all neuron classes are summarized in Fig. 3(h) as functions of $W_{SOM\text{-}PV}$. Pyr neurons and SOM interneurons were activated with increasing $W_{SOM\text{-}PV}$, whereas the opposite modulation pattern was observed in the other 2 neuron classes. Activated SOM interneurons directly inhibited PV interneuron activity. As $W_{SOM\text{-}PV}$ increased, activated SOM interneurons seemed to have a greater influence on Pyr neuron responses. Notably, the STH power between 20 and 30 Hz in the cortical microcircuit was

markedly enhanced via the coactivation of Pyr neurons and SOM interneurons (Fig. 3(i)); this finding appears to be consistent with physiological results from the rodent V1 (Roopun et al. 2010; Chen et al. 2017; Veit et al. 2017). Additionally, the magnitude of gamma-band activity was slightly increased by the activation of interactions between Pyr neurons and SOM interneurons. When the broad range of Pyr neuron STH power increased, PV interneuron rates were reduced by the activation of interactions between Pyr neurons and SOM interneurons.

Synaptic delay between specific cell subtypes for the modulation of responses and synchronized oscillations in the cortical microcircuit

The responses and oscillatory characteristics of neuronal microcircuits are significantly modulated by synaptic delays between neuron classes (Teramae et al. 2012). To analyze the contributions of specific neuron classes and subtypes to the modulation of responses and synchronized oscillations in our model, we performed simulations with various synaptic delays from Pyr to PV ($d_{\text{Pyr-PV}}$), from Pyr to SOM ($d_{\text{Pyr-SOM}}$), from SOM to PV ($d_{\text{SOM-PV}}$), and between Pyr neuron populations ($d_{\text{Pyr-Pyr}}$). Spike raster plots, population rates, and characteristics of the synchronized oscillations for our model with various synaptic delays are summarized in Fig. 4. In these simulations, we applied visual stimuli to all neuron classes.

Simulations of our model with various $d_{\text{Pyr-PV}}$ suggest that SOM interneuron activation is critical for both the increased STH power of Pyr neurons and the preferential generation of beta-band (20–30 Hz) activity. Spike raster plots of Pyr neurons for $d_{\text{Pyr-PV}}$ of 1.0 and 4.0 ms are displayed in Fig. 4(a). The spiking density and window of Pyr neurons were markedly modulated by these synaptic delays. The influence of $d_{\text{Pyr-PV}}$ on the population rates of all neuron classes and on the STH power of Pyr neurons are shown in Fig 4(b) and (c), respectively. Decreasing $d_{\text{Pyr-PV}}$ from 2 to 1 ms strongly reduced the magnitude of beta-band activity in the range between 20 and 30 Hz (red line in Fig. 4(c)), with no marked modulation of the population rates of any neuron classes (Fig. 4(b)). By contrast, slower synaptic delays (4 ms) not only substantially activated SOM interneurons (Fig. 4(b)) but also increased the magnitude of the whole range of STH power in Pyr neurons (blue line in Fig. 4(c)). In this condition, PV interneurons might be slightly activated. Therefore, the influence of markedly activated SOM interneurons on Pyr neuron responses seemed to be more dominant than that of the original model (black line in Fig. 4(c)). In addition, activated SOM interneurons might modulate the time course characteristics of PV interneurons. In particular, the coactivation of Pyr neurons and SOM interneurons preferentially facilitated the magnitude of beta-band activity for the range between 20 and 30 Hz; this finding appears consistent with physiological reports (Roopun et al. 2010; Chen et al. 2017; Veit et al. 2017).

Next, we performed simulations with various $d_{\text{Pyr-SOM}}$. These simulations indicated a contribution of transmission speeds from Pyr neurons to SOM interneurons in visually induced beta oscillation generation in the cortical microcircuit of layers 2/3. Figure 4(d) shows the spike raster plots of Pyr neurons for $d_{\text{Pyr-SOM}}$ of 0.3 and 12 ms. The large increase of $d_{\text{Pyr-SOM}}$ to 12 ms widened the intervals of synchronized oscillation in Pyr neurons (bottom panel of Fig. 4(d)). However, the population rates for each neuron class were only minimally altered by changing $d_{\text{Pyr-SOM}}$ from 0.3 to 12 ms (Fig. 4(e)). Nonetheless, a longer synaptic delay ($d_{\text{Pyr-SOM}}$ of 12.0 ms) shifted the peak location in the STH power of Pyr neurons toward the left (blue line in Fig. 4(f)). Additionally, rapid transmission from Pyr neurons to SOM interneurons ($d_{\text{Pyr-SOM}} = 0.3$ ms) decreased the magnitude of beta-band activity (red line in Fig. 4(f)).

Simulation results of our model with various $d_{\text{SOM-PV}}$ suggested that markedly delayed synapses from SOM to PV interneurons increase the magnitude of beta-band activity. Figure 4(g) shows the spike raster plots of Pyr neurons for $d_{\text{SOM-PV}}$ of 0.5, 4.0, and 8.0 ms. The spiking density and window of Pyr neurons were markedly modulated from $d_{\text{SOM-PV}}$ of 4.0–8.0 ms. However, the population rates of all neuron classes were generally unchanged by $d_{\text{SOM-PV}}$ (Fig. 4(h)). The STH power for various $d_{\text{SOM-PV}}$ is shown in Fig. 4(i). When we used relatively slow transmission from SOM to PV interneurons ($d_{\text{SOM-PV}} = 8.0$ ms), the magnitude of beta-band activity was markedly increased (blue line in Fig. 4(i)) and there was a slight increase of gamma-band activity from 50 Hz. Thus, markedly delayed synapses from SOM interneurons might modulate the rhythm of synchronized responses in PV interneurons, which may then induce beta oscillation in Pyr neurons.

Simulations of our model indicated that synaptic delays between excitatory neurons, in addition to the distribution of synaptic strengths, might be essential for determining the characteristics of synchronized oscillations in the cortical microcircuit. Interconnections between excitatory neurons strongly influence the activity in neuronal microcircuits (Teramae et al. 2012; Nobukawa, Nishimura, et al. 2021a; Nobukawa, Wagatsuma, et al. 2021b). We thus investigated how interactions between Pyr neurons might modulate the neuronal responses in layers 2/3 of the V1 via simulations with various $d_{\text{Pyr-Pyr}}$ (Fig. 4(j)–(l)). Spike raster plots of Pyr neurons for $d_{\text{Pyr-Pyr}}$ of 1, 4, and 8 ms are shown in Fig. 4(j). Regardless of $d_{\text{Pyr-Pyr}}$, we observed synchronous and rhythmical responses in Pyr neurons. In addition, the spike intervals of Pyr neurons were shortened with increasing $d_{\text{Pyr-Pyr}}$. Figure 4(k) illustrates the population rates of all neuron classes as functions of $d_{\text{Pyr-Pyr}}$. The population rates of all neuron classes were almost constant when $d_{\text{Pyr-Pyr}}$ was increased, whereas rapid transmission between Pyr neurons ($d_{\text{Pyr-Pyr}} = 1$ ms) activated Pyr neurons and PV and SOM interneurons. Furthermore, rapid transmission between Pyr neurons increased the magnitudes of the whole range of STH power in Pyr neurons (red line in Fig. 4(l)). By contrast, there were 2 peaks in STH power under slower synaptic transmission simulations, such as with $d_{\text{Pyr-Pyr}}$ of 4 and 8 ms (green and blue lines, respectively, in Fig. 4(l)).

Roles of synaptic strengths and delays from VIP to SOM interneurons for attentional modulation in layers 2/3 of the V1

In our model, attentional modulation in the cortical microcircuit occurred via disinhibition, which was based on connections from VIP to SOM interneurons (Fig. 1(a)). To better understand the mechanism of attentional modulation in the V1, we applied the model with various synaptic strengths ($W_{\text{VIP-SOM}}$) and lengths ($d_{\text{VIP-SOM}}$) from VIP to SOM interneurons. In these simulations, in addition to applying feedforward inputs, we provided feedback signals (mediating selective attention) to VIP interneurons. The simulation results for various $W_{\text{VIP-SOM}}$ and $d_{\text{VIP-SOM}}$ are summarized in Fig. 5.

Spike raster plots of Pyr neurons for $W_{\text{VIP-SOM}}$ of 0.5 and 2.0 are shown in Fig. 5(a). Pyr neuron activity was strongly modulated by $W_{\text{VIP-SOM}}$. In addition, $W_{\text{VIP-SOM}}$ modulated the density and rhythm of synchronized activity in Pyr neurons. Figure 5(b) shows the population rates of Pyr neurons and all interneuron subtypes as a function of $W_{\text{VIP-SOM}}$. With increasing $W_{\text{VIP-SOM}}$, Pyr neurons and PV and VIP interneurons were excited, whereas SOM interneurons

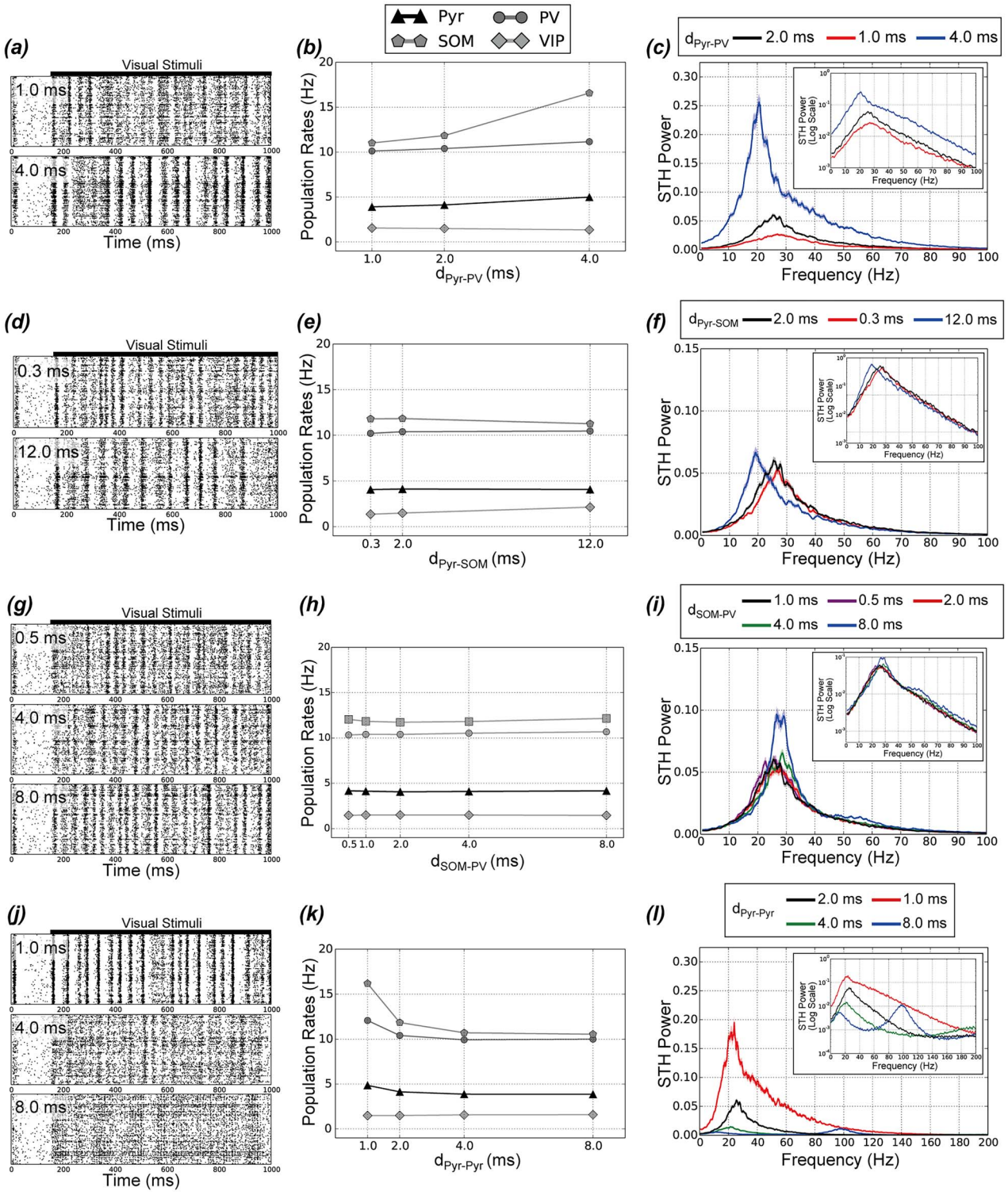

Fig. 4. Effects of synaptic delay on activity in the proposed microcircuit model. Panels (a–c), (d–f), (g–h), and (j–l) demonstrate the responses with various synaptic delays from Pyr to PV (d_{Pyr-PV}), from Pyr to SOM ($d_{Pyr-SOM}$), from SOM to PV (d_{SOM-PV}), and from Pyr to Pyr ($d_{Pyr-Pyr}$), respectively. Background inputs and visual stimuli were presented to the model during these simulations. All conventions are the same as those in Fig. 3. a) Raster plots showing all spike trains of the Pyr neurons for various d_{Pyr-PV}. The top and bottom panels present the simulation results with d_{Pyr-PV} of 1.0 and 4.0 ms, respectively. b) The mean population firing rates of Pyr (triangles), PV (circles), SOM (pentagons), and VIP (squares) neurons in the microcircuit model as a function of d_{Pyr-PV}. This plot shows the averages of 50 simulation trials. c) STH power of Pyr neurons, averaged over 50 simulation trials, with d_{Pyr-PV} of 2.0 (black line), 1.0 (red line), and 4.0 (blue line) ms. the inset shows a log-scale plot of the same STH power results for Pyr neurons. d) Raster plots showing all spike trains of Pyr neurons with various $d_{Pyr-SOM}$. For these plots, $d_{Pyr-SOM}$ were set to 0.3 and 12.0 ms. e) Mean population firing rates (50 simulation trials) of each neuron class as functions of $d_{Pyr-SOM}$. f) STH power of Pyr neurons, averaged over 50 simulation trials, for various $d_{Pyr-SOM}$. These curves were obtained through simulations with $d_{Pyr-SOM}$ of 2.0 (black line), 0.3 (red line), and 12.0 (blue line) ms. g) Raster plots of Pyr neurons with various d_{SOM-PV}. The top, middle, and bottom panels represent Pyr neuron activity with d_{SOM-PV} of 0.5, 4.0, and 8.0 ms, respectively. h) The mean population rates (50 simulation trials) of the neuron classes as functions of d_{SOM-PV}. i) STH power of Pyr neurons, averaged over 50 simulations, for d_{SOM-PV} of 1.0

were inhibited. In our microcircuit model, SOM and VIP interneurons interacted with one another (Fig. 1(a)). In the simulation with $W_{VIP\text{-}SOM}$ of 0.5, VIP interneurons may have been significantly inhibited by SOM interneurons despite the projection of selective attention. Furthermore, the attentional effects of STH power for the gamma-band activity of Pyr neurons was not observed in the model simulation with $W_{VIP\text{-}SOM}$ of 0.5 (black solid line in Fig. 5(c); see also Fig. 2(c)). By contrast, attentional effects were enhanced by increasing $W_{VIP\text{-}SOM}$ (black dashed line in Fig. 5(c)). These results suggest the critical role of connections from VIP to SOM interneurons for attentional modulation in layers 2/3 of the V1.

Model simulations with various $d_{VIP\text{-}SOM}$ indicated that the speed of synaptic transmission from VIP to SOM interneurons is a key factor in achieving both attentional modulation of neuronal activity and synchronized oscillations in the cortical microcircuit of layers 2/3 in the V1. Spike raster plots of Pyr neurons for $d_{VIP\text{-}SOM}$ of 0.5 and 2 ms are shown in Fig. 5(d). As was observed in the population rates (Fig. 5(e)), Pyr neurons were activated when $d_{VIP\text{-}SOM}$ was decreased from 1.0 to 0.5 ms. In addition, the spike intervals of Pyr neurons were shortened with decreased $d_{VIP\text{-}SOM}$. Notably, more rapid synaptic transmission from VIP to SOM interneurons led to the activation of STH power in the low-gamma band (30–50 Hz) for Pyr neurons (black solid line in Fig. 5(f)), whereas the low-gamma band magnitude in Pyr neurons decreased when $d_{VIP\text{-}SOM}$ was increased from 1 (gray line in Fig. 5(f)) to 2 ms (black dashed line in Fig. 5(f)). These simulation results for the synaptic connections from VIP to SOM interneurons suggest that the rapid and marked inhibition from VIP to SOM interneurons is essential for inducing attentional modulation of activity in cortical layers 2/3 of the V1.

Discussion

In the present study, to investigate both the circuitry structure of cortical layers 2/3 in the V1 and the specific role of the main inhibitory interneuron subtypes PV, SOM, and VIP in the regulation of neuronal activity and synchronized oscillations for visual processing, we developed a computational microcircuit model with a biologically plausible structure (Fig. 1(a)). Simulations of our proposed model indicate that feedback signals mediating selective attention to VIP interneurons not only activate Pyr neurons and PV interneurons and suppress SOM interneurons but also modulate the strength of gamma-band activity (Fig. 2). The attention-induced enhancement of gamma-band activity is in agreement with physiological reports from the monkey visual cortex (Womelsdorf et al. 2006; Bosman et al. 2012). In addition, these results suggest the contribution of interactions between Pyr neurons and PV interneurons to the preferential generation of gamma oscillations in cortical layers 2/3 of the V1.

To better understand the functions of the distinct interneuron subtypes, we performed simulations of the microcircuit model with various synaptic weights and delays (Figs 3 and 4). A decrease in synaptic strength from Pyr neurons to PV interneurons markedly increased the magnitude of beta-band activity in Pyr neurons for the range between 20 and 30 Hz and activated SOM and inactivated PV interneurons. By contrast, when synaptic strengths from Pyr neurons to SOM interneurons were decreased, the magnitude of gamma-band activity of Pyr neurons between 30 and 80 Hz was markedly increased in addition to the activation of PV interneurons and the inactivation of SOM interneurons. These simulation results suggest that SOM and PV interneurons are critical for the generation of slow (20–30 Hz) and fast (30–80 Hz) oscillations, respectively. These specific roles of distinct interneuron classes appear consistent with recent physiological reports (Roopun et al. 2010;Chen et al. 2017; Veit et al. 2017). Compared with the findings using various synaptic strengths, we did not observe more marked modulations in the firing rates of Pyr neurons with various synaptic delays. However, the rhythms of synchronized responses in Pyr neurons were modulated by slower synapses both from Pyr to interneurons and between interneurons.

Our model also suggested that synaptic connections from VIP to SOM interneurons are critical for the attentional modulation of activity in cortical layers 2/3 of the V1 (Fig. 5). Our results indicate that rapid and strong inhibition from VIP to SOM interneurons is essential for inducing attentional modulation for low-gamma frequencies (30–50 Hz).

Different subtypes of inhibitory interneurons may engage the generation of distinct rhythms of oscillatory activity in the visual cortex

In our simulations, feedback signals (mediating selective attention) were provided to VIP interneurons (Fig. 1(a)); these not only activated Pyr neurons and PV and VIP interneurons (Fig. 2(a) and (b)) but also enhanced the magnitude of both low (30–50 Hz) and high (50–100 Hz) gamma-band activity (Fig. 2(c)). These observed attention-induced gamma oscillations are in agreement with physiological results for attentional modulations in the visual cortex (Womelsdorf et al. 2006). Additionally, the magnitude of gamma-band oscillations was significantly increased by coactivating both Pyr neurons and PV interneurons in addition to inhibiting SOM interneurons (Fig. 3(e) and (f)). These results imply that inhibitory PV interneurons are important for the generation of gamma-band oscillations in cortical layers 2/3 of the V1.

Our model predicted that the spiking of inhibitory SOM interneurons preferentially contributes to the generation of slow neuronal oscillations in cortical layers 2/3 of the V1. In contrast to the modulation patterns of synchronized oscillations based on PV interneuron activation, the activation of interactions between Pyr neurons and SOM interneurons increased the magnitude of the whole range of STH power in Pyr neurons (Fig. 3(b), (c), (h), and (i); Fig. 4(b) and (c)). Specifically, the activation of SOM interneurons was important for the preferential generation of beta oscillations (20–30 Hz). Of interest, although the rates of all neuron classes and subtypes were consistent across various durations of synaptic delay from SOM interneurons to Pyr neurons (Fig. 4(e)), an extreme increase in this delay modulated the magnitude of slow oscillatory activity (10–30 Hz; blue line in Fig. 4(f)).

Simulations with our model suggest that the different subtypes of inhibitory interneurons contribute to the generation of distinct frequency-band oscillations in layers 2/3, which is consistent with recent physiological results (Chen et al. 2017; Veit et al. 2017). The distinct actions of different interneuron subtypes on synchronized oscillations might arise from the neuron-subtype-specific

(black line), 0.5 (purple line), 2.0 (red line), 4.0 (green line), and 8.0 (blue line) ms, respectively. j) Raster plots of the Pyr neurons with various $d_{Pyr\text{-}Pyr}$. The top, middle, and bottom panels represent the simulation results with $d_{Pyr\text{-}Pyr}$ of 1.0, 4.0, and 8.0 ms, respectively. k) Mean population firing rates (50 simulation trials) of each neuron class as a function of $d_{Pyr\text{-}Pyr}$. l) STH power of the Pyr neuron population for various $d_{Pyr\text{-}Pyr}$. These curves were obtained through simulations with $d_{Pyr\text{-}Pyr}$ of 2.0 (black line), 1.0 (red line), 4.0 (green line), and 8.0 (blue line) ms.

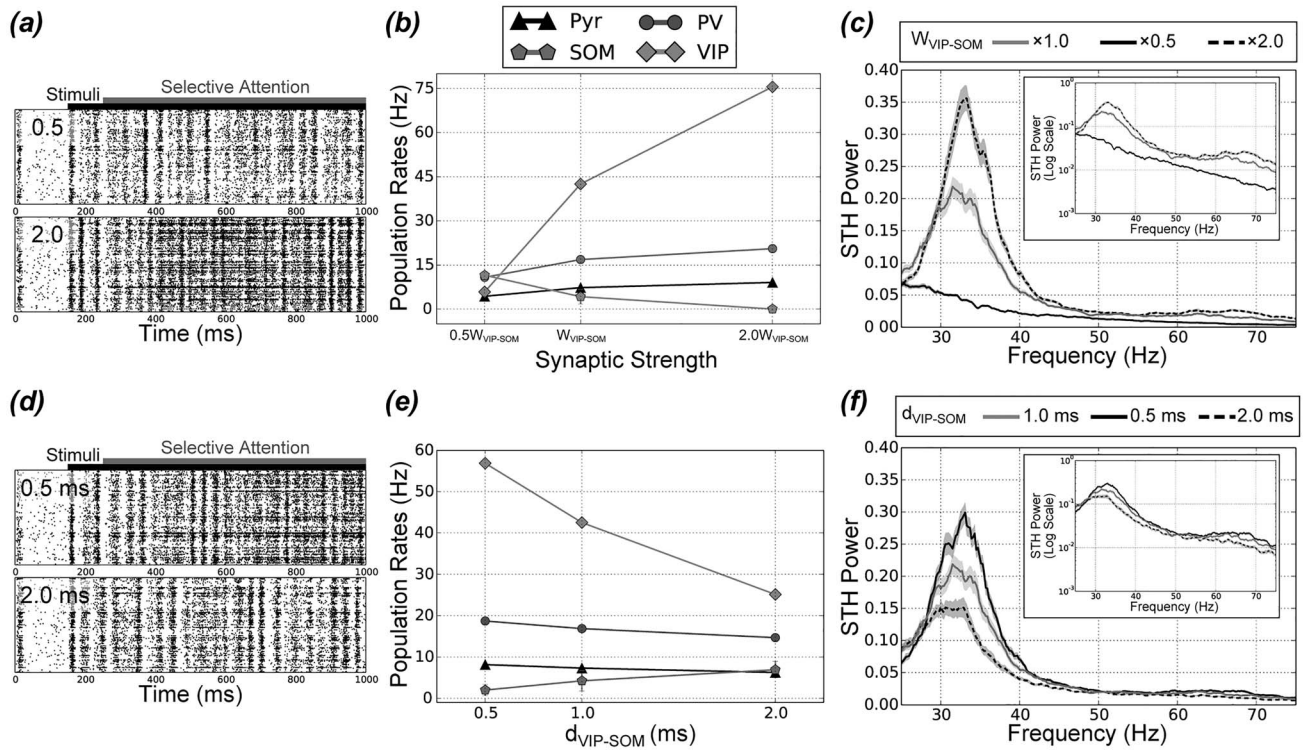

Fig. 5. Simulation results of the proposed microcircuit model with various synaptic strengths ($W_{VIP\text{-}SOM}$) and lengths ($d_{VIP\text{-}SOM}$). Panels (a–c) and (d–f) demonstrate the responses with various $W_{VIP\text{-}SOM}$ and $d_{VIP\text{-}SOM}$, respectively. In these simulations, we added selective attention as well as visual stimuli to VIP neurons. All conventions are the same as those in Figs 3 and 4. a) Raster plots showing all spike trains of Pyr neurons for various $W_{VIP\text{-}SOM}$. The top and bottom panels represent the simulation results with 0.5 and 2.0 × $W_{VIP\text{-}SOM}$, respectively. For these plots, selective attention was activated during the period represented by the gray bar at the top of the panel (250 ms–1 s). b) Mean population firing rates of Pyr (triangles), PV (circles), SOM (pentagons), and VIP (squares) neurons as functions of $W_{VIP\text{-}SOM}$ (based on 50 simulation trials). c) STH power of Pyr neurons, averaged over 50 simulation trials, versus $W_{VIP\text{-}SOM}$ (gray line), 0.5 × $W_{VIP\text{-}SOM}$ (solid black line), and 2.0 × $W_{VIP\text{-}SOM}$ (dashed black line). The inset shows a log-scale plot of the same STH power results of Pyr neurons. d) Raster plots showing all spike trains of Pyr neurons with various $d_{VIP\text{-}SOM}$ (0.5 and 2.0 ms). e) Mean population firing rates of each neuron class under the selective attention condition as a function of $d_{VIP\text{-}SOM}$. These were computed based on 50 simulation trials. f) Influence of $d_{VIP\text{-}SOM}$ on attentional modulation for the STH power of Pyr neurons. The gray, solid black, and dashed black lines correspond to the simulation results with $d_{VIP\text{-}SOM}$ of 1.0, 0.5, and 2.0 ms, respectively.

τ_m. In previous computational studies (Buehlmann and Deco 2008; Teramae et al. 2012), the characteristics of fast-spiking neurons were reproduced by using faster τ_m. Furthermore, a physiological study has reported that PV interneurons have much faster τ_m values than other neuron classes and subtypes (Neske et al. 2015; see also Table 2). The activation of interactions between excitatory neurons, such as Pyr neurons, and fast-spiking neurons, such as PV interneurons, might generate faster synchronized oscillations in the cortical microcircuit.

Previous network models of excitatory and inhibitory neurons have suggested the mechanisms and functions of gamma-band oscillations in layers 2/3 of the V1 (Jia et al. 2013; Han, Wang, et al., 2021b). However, it was difficult for these models to elucidate how slow neural oscillations are generated in the cortical microcircuit because they did not include diverse inhibitory neuron subtypes. By contrast, our model was based on current knowledge of cortical microcircuitry (Song et al. 2005; Lefort et al. 2009; Rudy et al. 2011; Teramae et al. 2012; Pfeffer et al. 2013; Potjans and Diesmann 2014; Neske et al. 2015; Lee et al. 2017, 2018) and included various neuron classes and subtypes that interacted with one another to regulate visual processing activity in layers 2/3 of the V1. Simulations of the model suggest that inhibitory signals from PV and SOM interneurons preferentially induce fast and slow synchronized oscillations, respectively, in cortical visual layers 2/3. The neuron-subtype-specific τ_m (Neske et al. 2015; Table 2) might be important for the generation of distinct frequency-band oscillations at least in part. Our model suggests how distinct frequency-band oscillations are generated in a cortical microcircuit in layers 2/3 of the V1. Thus, the findings of the current study provide clues regarding possible visual processing structures as well as mechanisms for the establishment and attentional modulation of visual perception.

Mechanism of attentional modulation in the cortical microcircuit in layers 2/3 of the V1

In the proposed model, VIP neurons mediated feedback signals (from higher cortical areas) and were important for replicating the attentional modulation that has been observed experimentally in local cortical circuits: VIP interneurons activated Pyr neurons and increased the magnitude of gamma-band activity (Fig. 2). In our model, this attentional modulation of Pyr neurons was induced by inhibiting the responses of SOM interneurons. Our network model included mutual interactions between VIP and SOM interneurons (Fig. 1(a); Zhang et al. 2014; Mardinly et al. 2016). Furthermore, inhibitory connections from VIP interneurons were restricted to SOM interneurons. Activation of VIP interneurons arising from selective attention preferentially inhibited SOM interneurons, which activated the interactions between excitatory Pyr neurons and fast-spiking PV interneurons (Fig. 2(a) and (b)). As discussed in the previous section, the coactivation of Pyr

neurons and PV interneurons contributed to gamma-band oscillation generation in the cortical microcircuit. Local disinhibition by connections from VIP to SOM interneurons might be a plausible mechanism for the attentional modulation of responses in the cortical microcircuit in layers 2/3 of the V1.

Simulations of our model indicate that $d_{\text{VIP-SOM}}$ is a key factor in the attentional modulation of responses in cortical layers 2/3 (Fig. 5(d)–(f)). Increases in $d_{\text{VIP-SOM}}$ increased the population rates of SOM interneurons, which then inhibited the responses of Pyr neurons and PV interneurons (Fig. 5(e)). Thus, in our model, SOM interneurons might regulate microcircuit responses by transmitting their signals to all other neuron populations. Additionally, as discussed previously and reported in an earlier study (Veit et al. 2017), the spiking of inhibitory SOM interneurons is important for the generation of various ranges of synchronized oscillations. These results suggest a critical role for SOM interneurons in inducing the attentional modulation of responses and synchronized oscillations in the V1.

As discussed in the previous and present sections, simulations of our model indicated the role of selective attention in inducing gamma-band oscillations. In the current study, external inputs (visual stimuli and selective attention) were described using independent Poisson spike trains. However, feedback signals in the beta-band frequency have been observed in a variety of sensory systems (Wang 2010). In addition, neuronal activity at beta and gamma frequencies might interact with one another during visual processing and selective attention. In a physiological study, Richter et al. (2017) reported that interactions between feedback signals from the parietal area 7a to the V1 and feedforward stimulus-induced processing from the V1 to the V4 enhance responses to a selected stimulus. In their experiments, the feedforward inputs of a visual stimulus seemed to be subserved by interareal gamma-band oscillations, whereas feedback signals might have been mediated by beta-band activity. In a computational study, Lee et al. (2013) applied feedback signals mediating selective attention to the layered cortical microcircuit model of sensory cortical areas. In their model, top-down signals were synchronized, oscillated at beta-band frequency, and were projected to the layer 5; this increased the gamma-band frequency power at layers 2/3. On the basis of these findings, simulations of the current model using inputs with various oscillatory rhythms might provide insights into the mechanisms of attention-induced oscillatory activity for establishing visual perception.

Distributions of synaptic conductance strength between Pyr neurons for modulating the cortical microcircuit responses

In our microcircuit model, synaptic strengths between excitatory Pyr neurons were distributed according to a long-tailed, log-normal distribution (Song et al. 2005; Lefort et al. 2009; Teramae et al. 2012; Nobukawa, Nishimura, et al. 2021a; Nobukawa, Wagatsuma, et al. 2021b). This log-normal distribution of synaptic strength between excitatory neurons seems to be critical for determining the spatiotemporal characteristics of neural activity and the functions of cortical networks (Hiratani et al. 2013; Omura et al. 2015). Our previous study indicated the important contribution of sparsely distributed, strong synapses to the generation of neural dynamics (Nobukawa, Wagatsuma, et al. 2021b). In this previous work, we performed simulations of the model, which consisted of excitatory and inhibitory neuron populations with log-normally distributed excitatory-to-excitatory connections (although very strong synapses between excitatory neurons were removed). Interestingly, the temporal dynamics of the model responses in the absence of strong excitatory-to-excitatory synaptic connections were determined by the rhythm of external periodic inputs more than when there were sparse, strong synapses between excitatory neurons. Furthermore, in another study (Nobukawa, Nishimura, et al. 2021a), we applied gamma distribution—a typical but different long-tailed distribution—to the network model of excitatory and inhibitory neurons to investigate the influence of synaptic connections within the excitatory population. The behaviors of this previous model were similar to those of the model in which excitatory-to-excitatory synapses followed a log-normal distribution. In addition, the findings of the current study suggest that synaptic delays as well as strengths between excitatory neurons are important for the behaviors of model responses (Fig. 4(j)–(l)). Further computational studies of synaptic connections and delays between excitatory neurons are needed to better understand the mechanism underlying the generation of oscillatory rhythms in neuronal networks.

Discrepancies between physiological experiments and model simulations

The neural mechanisms and functional role of the stimulus-evoked oscillations that were generated in our model require further investigation. Simulations with our microcircuit model suggest that visual stimuli contribute to the generation of neural activity with beta oscillation, whereas selective attention has a key role in eliciting synchronized oscillations with gamma-band activity in layers 2/3 of the V1. Previous physiological studies have reported an increased neuronal activity of gamma-band oscillations in the visual cortex caused by selective attention (Womelsdorf et al. 2006; Bosman et al. 2012). Interestingly, both visually and optogenetically induced oscillations of gamma-band activity modulate the gain of spike responses to task-related stimuli and directly impact behavioral response times in animals (Ni et al. 2016; Rohenkohl et al. 2018). However, in these previous studies, neuronal responses were recorded using LFPs. During neuronal recording, 2 visual stimuli were presented to animals at distinct locations within their visual field. Under these experimental conditions, animals attended to a target stimulus or its spatial location. Additionally, coherence between spikes and LFPs were analyzed to link synchronized neural oscillatory activity with behaviors. Thus, an extension of our model is necessary to understand the detailed mechanisms that generate synchronized oscillations under conditions consistent with these experiments.

As discussed previously, to physiologically analyze the characteristics of neural oscillations during visual perception and selective attention, LFP has been used to measure the responses of neuronal populations (Womelsdorf et al. 2006; Bosman et al. 2012; Ni et al. 2016; Rohenkohl et al. 2018). In the current study, to reduce computational costs, we used STHs of Pyr neurons as a model of LFP based on previous studies (Buia and Tiesinga 2008; Lee et al. 2018). However, the mechanisms and nature of LFP are still relatively unknown (Lindén et al. 2011). To analyze the activity of a network model, Buehlmann and Deco (2008) used 3 different methods to compute LFP signals, which were based on spike rates, membrane potentials, and incoming synaptic currents. These 3 measurements of LFP signals highly correlated in their study. In addition, they reported that their qualitative results did not depend on the LFP computational methods. Results from another computational study suggest that a linear combination of excitatory and inhibitory synaptic currents that arise from a network

based on spiking model neurons can capture the time course characteristics of LFP (Mazzoni et al. 2015). However, further analyses of a detailed model of LFP may be necessary to further understand the distinct roles of specific interneuron subtypes.

Some discrepancies between our simulations and previous experiments may arise from the main limitation of our model: It did not include experimentally observed interactions among cortical microcircuits with different receptive fields. However, our simulations suggested that SOM interneurons contribute to the generation of neuronal activity with beta oscillations, which is consistent with the physiological reports of visual areas in rodents (Chen et al. 2017; Veit et al. 2017). In the rodent visual cortex, both SOM interneuron responses and beta oscillation magnitudes increase with an increase in the size of visual stimuli. Horizontal connections across receptive fields have been proposed as the mechanism underlying such stimulus-size-dependent modulations (Ayaz et al. 2013; Vaiceliunaite et al. 2013). Furthermore, in the cat V1, many excitatory neurons in superficial layers have axons that project horizontally over large distances (Gilbert and Wiesel 1979; Rockland and Pandya 1979; Gilbert and Wiesel 1983; Hirsch and Gilbert 1991), which might induce surround modulation of visual activity (Malach et al. 1993). Adesnik et al. (2012) proposed a plausible cortical circuit mechanism for surround modulation in visual responses: via long-range horizontal connections from Pyr neurons to SOM interneurons. The resultant modulatory effect seems to agree with concomitant modulations of physiological responses in SOM interneurons and increased beta oscillation magnitudes in the visual cortex of rodents. However, in our current model, no interactions occurred between units with different receptive fields. Therefore, SOM interneurons did not receive external excitatory signals from their surrounding receptive fields. The mechanisms and characteristics of long-range horizontal connections have been investigated in various animals and cortical areas (Albowitz and Kuhnt 1993; Aroniadou and Keller 1993; McDonald and Burkhalter 1993; Lohmann and Rörig 1994; Ozeki et al. 2009; Van den Bergh et al. 2010; Ayaz et al. 2013; Vaiceliunaite et al. 2013; Self et al. 2014; Wang et al. 2020). However, it remains to be explored how these surrounding effects across receptive fields modify the dynamics of cortical microcircuits.

Projections of visual stimuli to our microcircuit model induced synchronized oscillatory responses in Pyr neurons (Fig. 2). However, visual stimulation has been reported to shift the V1 network toward a more asynchronous state (Tan et al. 2014). Therefore, visual stimulus-induced asynchronous activity possibly arises from a tight balance between excitatory and inhibitory inputs to neurons (Ahmandian and Miller, 2021). By contrast, in simulations of our model with visual stimuli, excitatory synaptic currents to some Pyr neurons seemed to be more dominant compared with inhibitory inputs, likely because excitatory synaptic weights between Pyr neurons obeyed a long-tailed, log-normal distribution (Teramae et al. 2012; Nobukawa, Nishimura, et al. 2021a; Nobukawa, Wagatsuma, et al. 2021b). Because of the long-tailed distribution of synaptic strengths between Pyr neurons, the small numbers of synapses induced marked depolarization and activation of postsynaptic Pyr neurons. In addition, in the biological V1, inhibitory neurons in layer 4 of the V1 seem to project to neuronal populations in layers 2/3 (Thomson et al. 2002; Wagatsuma et al. 2011; Potjans and Diesmann 2014). For simplicity, however, we applied only excitatory external inputs to our network. Further analysis of the balance between excitatory and inhibitory inputs to model neurons will provide insights into neuronal dynamics in layers 2/3 of the V1.

Differences among animal species in microcircuit structure and the generation of synchronized oscillations

Differences in cortical microcircuit structure among species may be important for our proposed model. Because it is difficult to obtain all necessary data from the literature on a single animal species, we constructed a biologically plausible structure of the cortical microcircuit model in layers 2/3 of the V1 (Fig. 1(a)), which was based on experimental data obtained from a range of animal species, such as the cat V1 (Binzegger et al. 2004), cat and rat cortices (Thomson et al. 2002; Thomson and Morris 2002), mouse visual cortex (Pfeffer et al. 2013), and mouse barrel cortex (Neske et al. 2015). However, we assume that the cortical microcircuit structure and the scale of its network are different among animal species. In addition, most recent experimental studies have reported the properties of PV, SOM, VIP inhibitory interneurons in rodents (Pfeffer et al. 2013; Neske et al. 2015; Jackson et al. 2016); it remains unclear whether these interneuron properties are consistent with those in the monkey V1.

Neural activity with synchronized oscillations has been observed in the V1 of various animal species. However, species-specific properties have also been reported (see the review by Han, Shapley, et al. (2021a)). In the macaque and cat, visual-stimulus-induced gamma-band oscillations are generated in layers 2/3 of the V1 and not in the lateral geniculate nucleus (Han, Wang, et al. 2021b; Roberts et al. 2013; van Kerkoerle et al. 2014). By contrast, in mice, gamma-band activity generated in subcortical regions, including the lateral geniculate nucleus and retina, is projected to input layers of the V1 (Saleem et al. 2017; Storchi et al. 2017; Schneider et al. 2021). These findings suggest that the mechanisms underlying synchronized oscillation generation in the visual cortex are distinct among different animal species. Further studies of species differences are therefore necessary to better understand the mechanisms and roles of oscillatory activity rhythms.

The responses in our model simulations were in good agreement with prior physiological results of both attentional modulation (Womelsdorf et al. 2006; Bosman et al. 2012) and the specific roles of distinct interneuron subtypes for the generation of specific bands of synchronized oscillations (Chen et al. 2017; Lee et al. 2018). However, the neuronal responses of these physiological experiments were recorded from different animal species. The effects of attentional modulation on firing rates (McAdams and Maunsell 1999; Martinez-Trujillo and Treue 2004) and oscillatory activity (Womelsdorf et al. 2006; Bosman et al. 2012) were observed in the monkey visual cortex. By contrast, recent physiological studies of the mouse V1 indicated the specific roles of PV and SOM inhibitory interneurons for the generation of gamma- and beta-band oscillations, respectively (Chen et al. 2017; Lee et al. 2018). However, as discussed previously, both microcircuit structure and the mechanisms underlying oscillatory activity generation might be different among animal species. Although the experimental data that are currently available for constructing microcircuits of the V1 and to validate the simulation results of our model are limited, differences between species might be important and should be further investigated.

Possible extensions of the microcircuit model and limitations of the present model

The current version of our model describes the circuit structure of layers 2/3 in the V1 only. However, this is a clear oversimplification. Functional microcircuit units of the V1 for cortical

information processing have a 6-layered network with excitatory neurons and various inhibitory interneuron subtypes (Thomson et al. 2002; Thomson and Morris 2002; Binzegger et al. 2004; Billeh et al. 2020); this structure seems to be preserved across all neocortical regions. Visual perception is established via intra- and interlaminar information flow within a layered microcircuit (Franken and Reynolds 2021). Previous computational studies have proposed layered microcircuit models of the visual cortex to explore how different inputs interact with one another within the laminar structure to produce the neural modulations that are observed in visual areas (Wagatsuma et al. 2011, 2013; Lee et al. 2013, 2017; Potjans and Diesmann 2014; Schmidt et al. 2018). In addition, physiological studies in the monkey V1 have reported the laminar dependence of spike synchrony (Smith et al. 2013) and the roles of the different cortical layers in perceiving the figural region from the background (Self et al. 2013; van Kerkoerle et al. 2014; Poort et al. 2016). Thus, further studies of the complex interactions between various signals within the layered microcircuit of primates might be necessary to better understand the neural mechanisms of visual perception. Moreover, an extended network model with a detailed layered structure will provide greater insight into the mechanisms of sensory processing, and particularly attentional modulation, in cortical layers 2/3.

The present model consisted of a single cortical microcircuit processing a single receptive field only, which limits the validity of its predictions. During the model simulations, we applied 3 types of external inputs: background inputs, feedforward inputs (representing visual stimuli), and feedback signals (mediating selective attention). Background inputs were necessary for inducing and preserving spontaneous activity in our microcircuit model, whereas the feedforward inputs and feedback signals modulated neuronal responses and oscillations. However, the cortical microcircuit in layers 2/3 also includes rich recurrent synaptic connections within the same layer (Callaway 1998), which might be important for integrating various inputs to establish visual perception (Adesnik and Scanziani 2010; Noudoost et al. 2010; Self et al. 2013; Jia et al. 2013; Han, Wang, et al. 2021b). In addition, as discussed in previous sections, neuronal responses in the visual cortex are suppressed when stimuli with their preferred visual features are provided around their receptive fields (i.e. surround suppression) (Allman et al. 1985; Knierim and Van Essen 1992; Jones et al. 2001, 2002; Ozeki et al. 2009). Physiological studies have proposed that neural suppression in early vision, which occurs via interactions between receptive fields, is mainly mediated by long-distance horizontal connections from excitatory neurons to inhibitory SOM interneurons (Adesnik et al. 2012; Self et al. 2014; Chen et al. 2017). Additionally, a computational and physiological study of the monkey V1 indicated that slow (rather than fast) suppression activates surround suppression in output layers such as layers 2/3 of the V1 (Wang et al. 2020). We therefore need to extend the current model by including multiple processing units with mutual interactions across their receptive fields and to further clarify the roles of specific interneuron subtypes in regulating cortical microcircuit responses.

The present model with a single functional unit did not allow the investigation of interactions among cortical microcircuits sharing a common receptive field. Neurons in the V2 respond strongly to a bar presented in their receptive field if the bar is aligned with their preferred orientation (Reynolds et al. 1999). However, this neuronal response is markedly suppressed if the bar is accompanied by a second bar in a nonpreferred orientation, which implies that neuronal microcircuits with shared receptive fields interact with one another. Computational studies have suggested that such interactions among neuronal microcircuits with shared receptive fields occur via horizontal connections from excitatory to inhibitory neurons (Wagatsuma et al. 2011, 2013). Because our cortical microcircuit model described a single functional unit with a single orientation selectivity, it was unable to produce interactions among multiple microcircuits sharing a common receptive field. To add this feature to our model, we first need to know which subtype of inhibitory interneurons primarily mediates the local interactions between cortical microcircuits sharing a common receptive field. Thus, further experimental studies are needed to clarify the network mechanisms of intermicrocircuit interactions and their roles in visual perception.

Many studies have focused on the characteristics and functions of interneuron subtypes in the integration of various neural signals and the regulation of neuronal activity (Adesnik and Scanziani 2010; Adesnik et al. 2012; Pfeffer et al. 2013; Zhang et al. 2014; Neske et al. 2015; Mardinly et al. 2016). However, different conclusions have been reached regarding the function of PV and SOM interneurons in orientation tuning in the visual cortex: Some studies have reported that SOM interneuron activation increases orientation selectivity, whereas PV interneuron activation contributes very little to orientation tuning (Atallah et al. 2012; Wilson et al. 2012). By contrast, another study concluded that PV but not SOM interneurons contribute to the sharpness of orientation tuning (Lee et al. 2012). Future extensions of our microcircuit model may be able to explain these discrepancies between experimental observations. We have computationally studied the mechanisms of attentional modulation for orientation tuning in the V1 through simulations of a layered microcircuit model (Wagatsuma et al. 2013). In this model, the functional units for orientation selectivity interacted with one another via horizontal connections from excitatory to inhibitory neurons in layers 2/3. Thus, implementing intermicrocircuit interactions in the current model might provide insights into the interneuron subtypes that produce neural functions.

Acknowledgements

We thank Dr. Tomoki Kurikawa for valuable discussions. We thank Bronwen Gardner, PhD, from Edanz (https://jp.edanz.com/ac) for editing a draft of this manuscript.

Funding

This work was partly supported by the Japanese Society for the Promotion of Science (JSPS) (KAKENHI Grants 19K12737, 17K12704, and 20H04487 to NW and 22K12183 to SN).

Conflict of interest statement: The authors have declared that no conflict of interests exist.

Data and code availability

The data underlying this article areavailable in Figshare at https://figshare.com, and can be accessed with https://doi.org/10.6084/m9.figshare.20934352

References

Adesnik H, Scanziani M. Lateral competition for cortical space by layer-specific horizontal circuits. *Nature*. 2010:464:1155–1160. https://doi.org/10.1038/nature08935.

Adesnik H, Bruns W, Taniguchi H, Huang ZJ, Scanziani M. A neural circuit for spatial summation in visual cortex. *Nature*. 2012:490: 226–231. https://doi.org/10.1038/nature11526.

Aertsen A, Arndt M. Response synchronization in the visual cortex. *Curr Opin Neurobiol*. 1993:3:586–594. https://doi.org/10.1016/0959-4388(93)90060-C.

Ahmandian Y, Miller KD. What is the dynamical regime of cerebral cortex? *Neuron*. 2021:109:3373–3391. https://doi.org/10.1016/j.neuron.2021.07.031.

Albowitz B, Kuhnt U. The contribution of intracortical connections to horizontal spread of activity in the neocortex as revealed by voltage sensitive dyes and a fast optical recording method. *Eur J Neurosci*. 1993:5(10):1349–1359. https://doi.org/10.1111/j.1460-9568.1993.tb00921.x.

Allman J, Miezin F, McGuinness E. Stimulus specific responses from beyond the classical receptive field: neurophysiological mechanisms for local-global comparisons in visual neurons. *Annu Rev Neurosci*. 1985:8:407–430. https://doi.org/10.1146/annurev.ne.08.030185.002203.

Aroniadou VA, Keller A. The patterns and synaptic properties of horizontal intracortical connections in the rat motor cortex. *J Neurophysiol*. 1993:70(4):1553–1569. https://doi.org/10.1152/jn.1993.70.4.1553.

Atallah BV, Bruns W, Carandini M, Scanziani M. Parvalbumin-expressing interneurons linearly transform cortical responses to visual stimuli. *Neuron*. 2012:73:159–170. https://doi.org/10.1016/j.neuron.2011.12.013.

Ayaz A, Saleem AB, Schölvinck ML, Carandini M. Locomotion controls spatial integration in mouse visual cortex. *Curr Biol*. 2013:23(10): 890–894. https://doi.org/10.1016/j.cub.2013.04.012.

Bastos AM, Vezoli J, Bosman CA, Schoffelen JM, Oostenveld R, Dowdall JR, DeWeerd P, Kennedy H, Fries P. Visual areas exert feedforward and feedback influences through distinct frequency channels. *Neuron*. 2015:85:390–401. https://doi.org/10.1016/j.neuron.2014.12.018.

Billeh YN, Cai B, Gratiy SL, Dai K, Iyer R, Gouwens NW, Abbasi-Asl R, Jia X, Siegle JH, Olsen SR, et al. Systematic integration of structural and functional data into multi-scale models of mouse primary visual cortex. *Neuron*. 2020:106:388–403. https://doi.org/10.1016/j.neuron.2020.01.040.

Binzegger T, Douglas RJ, Martin KAC. A quantitative map of the circuit of cat primary visual cortex. *J Neurosci*. 2004:24:8441–8453. https://doi.org/10.1523/JNEUROSCI.1400-04.2004.

Bosman CA, Schoffelen JM, Brunet N, Oostenveld R, Bastos AM, Womelsdorf T, Rubehn B, Stieglitz T, de Weerd P, Fries P. Attentional stimulus selection through selective synchronization between monkey visual areas. *Neuron*. 2012:75:875–888. https://doi.org/10.1016/j.neuron.2012.06.037.

Buehlmann A, Deco G. The neural basis of attention: rate versus synchronization modulation. *J Neurosci*. 2008:28:7679–7689.

Buia CI, Tiesinga PH. Roles of interneuron diversity in the cortical microcircuit for attention. *J Neurophysiol*. 2008:99:2158–2182.

Callaway EM. Local circuits in primary visual cortex of the macaque monkey. *Annu Rev Neurosci*. 1998:21:47–74.

Cardin JA. Inhibitory interneurons regulate temporal precision and correlations in cortical circuits. *Trends Neurosci*. 2018:41:689–700.

Chen G, Zhang Y, Li X, Zhao X, Ye Q, Lin Y, Tao HW, Rasch MJ, Zhang X. Distinct inhibitory circuits orchestrate cortical beta and gamma band oscillations. *Neuron*. 2017:96:1403–1418. https://doi.org/10.1016/j.neuron.2017.11.033.

Deco G, Thiele A. Cholinergic control of cortical network interactions enables feedback-mediated attentional modulation. *Eur J Neurosci*. 2011:34:146–157.

Franken TP, Reynolds JH. Columnar processing of border ownership in primates visual cortex. *Elife*. 2021:10:e72573. https://doi.org/10.7554/eLife.72573.

Gilbert CD, Wiesel TN. Morphology and intracortical projections of functionally characterised neurons in the cat visual cortex. *Nature*. 1979:280:120–125. https://doi.org/10.1038/280120a0.

Gilbert CD, Wiesel TN. Clustered intrinsic connections in cat visual cortex. *J Neurosci*. 1983:3:1116–1133. https://doi.org/10.1523/JNEUROSCI.03-05-01116.1983.

Han C, Shapley R, Xing D. Gamma rhythms in the visual cortex: functions and mechanisms. *Cogn Neurodyn*. 2021a:16:745–756. https://doi.org/10.1007/s11571-021-09767-x.

Han C, Wang T, Wu Y, Li Y, Yang Y, Li L, Wang Y, Xing D. The generation and modulation of distinct gamma oscillations with local, horizontal, and feedback connections in the primary visual cortex: a model study on large-scale networks. *Neural Plast*. 2021b:2021:8874516. https://doi.org/10.1155/2021/8874516.

Herrero JL, Gieselmann MA, Sanayei M, Thiele A. Attention-induced variance and noise correlation reduction in macaque V1 is mediated by NMDA receptors. *Neuron*. 2013:78:729–739.

Hiratani N, Teramae JN, Fukai T. Associative memory model with long-tail-distributed hebbian synaptic connections. *Front Comput Neurosci*. 2013:6:102. https://doi.org/10.3389/fncom.2012.00102.

Hirsch JA, Gilbert CD. Synaptic physiology of horizontal connections in the cat's visual cortex. *J Neurosci*. 1991:11:1800–1809. https://doi.org/10.1523/JNEUROSCI.11-06-01800.1991.

Hoffmann JH, Meyer H-S, Schmitt J, Weitbrecht T, Sakmann B, Helmstaedter M. Synaptic conductance estimates of the connection between local inhibitor and pyramidal neurons in layer 2/3 of a cortical column. *Cereb Cortex*. 2015:25:4415–4429. https://doi.org/10.1093/cercor/bhv039.

Jackson J, Ayzenshtat I, Karnani MM, Yuste R. VIP+ interneurons control neocortical activity across brain states. *J Neurophysiol*. 2016:115:3008–3017. https://doi.org/10.1152/jn.01124.2015.

Jahr CE, Stevens CF. Voltage dependence of NMDA-activated macroscopic conductances predicted by single-channel kinetics. *J Neurosci*. 1990:10:3178–3182.

Jang HJ, Chung H, Rowland JM, Richards BA, Kohl MM, Kwang J. Distinct roles of parvalbumin and somatostatin interneurons in gating the synchronization of spike times in the neocortex. *Sci Adv*. 2020:6:eaay5333. https://doi.org/10.1126/sciadv.aay5333.

Jia X, Xing D, Kohn A. No consistent relationship between gamma power and peak frequency in macaque primary visual cortex. *J Neurosci*. 2013:33:17–25. https://doi.org/10.1523/JNEUROSCI.1687-12.2013.

Jones HE, Grieve KL, Wang W, Sillito AM. Surround suppression in primate V1. *J Neurophysiol*. 2001:86:2011–2028. https://doi.org/10.1152/jn.2001.86.4.2011.

Jones HE, Wang W, Sillito AM. Spatial organization and magnitude of orientation contrast interactions in primate V1. *J Neurophysiol*. 2002:88:2796–2808. https://doi.org/10.1152/jn.00403.2001.

Knierim JJ, Van Essen DC. Neuronal responses to static texture patterns in area V1 of the alert macaque monkey. *J Neurophysiol*. 1992:67:961–980. https://doi.org/10.1152/jn.1992.67.4.961.

Lee JH, Mihalas S. Visual processing mode switching regulated by VIP cells. *Sci Rep*. 2017:7:1843. https://doi.org/10.1038/s41598-017-01830-0.

Lee S-H, Kwan AC, Zhang S, Phoumthipphavong V, Flannery JG, Masmanidis SC, Taniguchi H, Huang ZJ, Zhang F, Boyden ES, et al. Activation of specific interneurons improves V1 feature selectivity and visual perception. *Nature*. 2012:488:379–383. https://doi.org/10.1038/nature11312.

Lee JH, Whittington MA, Kopell NJ. Top-down beta rhythms support selective attention via interlaminar interaction: a model. *PLoS Comput Biol*. 2013:9:e1003164. https://doi.org/10.1371/journal/pcbi.1003164.

Lee JH, Koch C, Mihalas S. A computational analysis of the function of three inhibitory cell types in contextual visual processing. *Front Comput Neurosci*. 2017:11:28. https://doi.org/10.3389/fncom.2017.00028.

Lee B, Shin D, Gross SP, Cho KH. Combined positive and negative feedback allows modulation of neuronal oscillation frequency during sensory processing. *Cell Rep*. 2018:25:1548–1560. https://doi.org/10.1016/j.celrep.2018.10.029.

Lefort A, Tomm C, Sarria J-CF, Petersen CCH. The excitatory neuronal network of the C2 barrel column in mouse primary somatosensory cortex. *Neuron*. 2009:61:301–316. https://doi.org/10.1016/j.neuron.2008.12.020.

Lindén H, Tetzlaff T, Potjans TC, Pettersen KH, Grün S, Diesmann M, Einevoll GT. Modeling the spatial reach of LFP. *Neuron*. 2011:72:859–872. https://doi.org/10.1016/j.neuron.2011.11.006.

Lohmann H, Rörig B. Long-range horizontal connections between supragranular pyramidal cells in the extrastriate visual cortex of the rat. *J Comp Neurol*. 1994:344(4):543–558. https://doi.org/10.1002/cne. 903440405.

Malach R, Amir Y, Harel M, Grinvald A. Relationship between intrinsic connections and functional architecture revealed by optical imaging and in vivo targeted biocytin injections in primate striate cortex. *Proc Natl Acad Sci U S A*. 1993:90:10469–10473. https://doi.org/10.1073/pnas.90.22.10469.

Mardinly AR, Spiegel I, Partizi A, Bazinet JE, Tzeng CP, Mandel-Brehm C, Harmin DA, Adesnik H, Fagiolini M, Greenberg ME. Sensory experience regulates cortical inhibitory by inducing IGl in VIP neurons. *Nature*. 2016:531:371–375. https://doi.org/10.1038/nature17187.

Martin AB, von der Heydt R. Spike synchrony reveals emergence of proto-objects in visual cortex. *J Neurosci*. 2015:35:6860–6870. https://doi.org/10.1523/JNEUROSCI.3590-14.2015.

Martinez-Trujillo JC, Treue S. Feature-based attention increases the selectivity of population responses in primate visual cortex. *Curr Biol*. 2004:14:744–751. https://doi.org/10.1016/j.cub.2004.04.028.

Mazzoni A, Lindén H, Cuntz H, Lansner A, Panzeri S, Einevoll GT. Computing the local field potential (LFP) from integrate-and-fire network models. *PLoS Comput Biol*. 2015:11(12):e1004584. https://doi.org/10.1371/journal.pcbi.1004584.

McAdams CJ, Maunsell HR. Effects of attention on orientation-tuning functions of single neurons in macaque cortical area V4. *J Neurosci*. 1999:19:431–441. https://doi.org/10.1523/JNEUROSCI.19-01-00431.

McDonald CT, Burkhalter A. Organization of long-range inhibitory connections with rat visual cortex. *J Neurosci*. 1993:13(2):768–781. https://doi.org/10.1523/JNEUROSCI.13-02-00768.1993.

Neske GT, Patrick SL, Connor BW. Contributions of diverse excitatory and inhibitory neurons to recurrent network activity in cerebral cortex. *J Neurosci*. 2015:35:1089–1105. https://doi.org/10.1523/JNEUROSCI.2279-14.2015.

Ni J, Wunderle T, Lewis CM, Desimone R, Diester I, Fries P. Gamma-rhythmic gain modulation. *Neuron*. 2016:92:240–251. https://doi.org/10.1016/j.neuron.2016.09.003.

Nobukawa S, Nishimura H, Wagatsuma N, Ando S, Yamanishi T. Long-tailed characteristic of spiking pattern alternation induced by log-normal excitatory synaptic distribution. *IEEE Trans Neural Netw Learn Syst*. 2021a:32:3525–3537. https://doi.org/10.1109/TNNLS.2020.3015208.

Nobukawa S, Wagatsuma N, Ikeda T, Hasegawa C, Kikuchi M, Takahashi T. Effect of steady-state response versus excitatory/inhibitory balance on spiking synchronization in neural networks with log-normal synaptic weight distribution. *Cogn Neurodyn*. 2021b:16:871–885. https://doi.org/10.1007/s11571-021-09757-z.

Noudoost B, Chang MH, Steinmetz NA, Moore T. Top-down control of visual attention. *Curr Opin Neurobiol*. 2010:20:183–190.

Omura Y, Carvalho MM, Inokuchi K, Fukai T. A lognormal recurrent network modle for burst generation during hippocampal sharp waves. *J Neurosci*. 2015:35:14585–14601. https://doi.org/10.1523/JNEUROSCI.4944-14.2015.

Ozeki H, Finn IM, Schaffer ES, Miller KD, Ferster D. Inhibitory stabilization of the cortical network underlies visual surround suppression. *Neuron*. 2009:62:578–592. https://doi.org/10.1016/j.neuron.2009.03.028.

Pfeffer CK. Inhibition neurons: vip cells hit the brake on inhibition. *Curr Biol*. 2014:24:R18–R20. https://doi.org/10.1016/j.cub.2013.11.001.

Pfeffer CK, Xue M, He M, Huang ZJ, Scanziani M. Inhibition of inhibition in visual cortex: the logic of connections between molecularly distinct interneurons. *Nat Neurosci*. 2013:16:1068–1076. https://doi.org/10.1038/nn.3446.

Pi HJ, Hangya B, Kvitsiani D, Sanders JI, Huang ZJ, Kepecs A. Cortical interneurons that specialize in disinhibitory control. *Nature*. 2013:503:521–524. https://doi.org/10.1038/nature12676.

Pillow JW, Shelens J, Paninski L, Sher A, Litke AM, Chichilnisky EJ, Simonccelli EP. Spatio-temporal correlations and visual signaling in a complete neuronal population. *Nature*. 2008:454:995–999. https://doi.org/10.1038/nature07140.

Poort J, Self MW, van Vugt B, Malkki H, Roelfsema PR. Texture segregation causes early figure enhancement and later ground suppression in area V1 and V4 of visual cortex. *Cereb Cortex*. 2016:26:3964–3976. https://doi.org/10.1093/cercor/bhv235.

Potjans TC, Diesmann M. The cell-type specific cortical microcircuit: relating structure and activity in a full-scale spiking network model. *Cereb Cortex*. 2014:24:785–806. https://doi.org/10.1093/cercor/bhs358.

Reynolds JH, Chelazzi L, Desimone R. Competitive mechanisms subserve attention in macaque areas V2 and V4. *J Neurosci*. 1999:19:1736–1753. https://doi.org/10.1523/JNEUROSCI.19-05-01736.1999.

Richter CG, Thompson WH, Bosman CA, Fries P. Top-down beta enhances bottom-up gamma. *J Neurosci*. 2017:37:6698–6711. https://doi.org/10.1523/JNEUROSCI.3771-16.2017.

Roberts MJ, Lowet E, Brunet NM, Wal MT, Tiesinga P, Fries P, Weerd PD. Robust gamma coherence between macaque V1 and V2 by dynamic frequency matching. *Neuron*. 2013:78:523–536. https://doi.org/10.1016/j.neuron.2013.03.003.

Rockland KS, Pandya DN. Laminar origins and terminations of cortical connections of the occipital lobe in the rhesus monkey. *Brain Res*. 1979:179:3–20. https://doi.org/10.1016/0006-8993(79)90485-2.

Rohenkohl G, Bosman CA, Fries P. Gamma synchronization between V1 and V4 improves behavioral performance. *Neuron*. 2018:100:953–963. https://doi.org/10.1016/j.neuron.2018.09.019.

Roopun AK, LeBeau FEN, Rammell J, Cunningham MO, Traub RD, Whittington MA. Cholinergic neuromodulation controls directed temporal communication in neocortex in vitro. *Front Neural Circuits*. 2010:4:8. https://doi.org/10.3389/fncir.2010.00008.

Rudy B, Fishell G, Lee S, Hjerling-Leffler J. Three groups of interneurons account for nearly 100% of neocortical GABAergic neurons. *Dev Neurobiol*. 2011:71:45–61. https://doi.org/10.1002/dneu.20853.

Saleem AB, Lien AD, Krumin M, Haider B, Rosón MR, Ayaz A, Reinhold K, Busse L, Carandini M, Harris KD. Subcortical source

and modulation of the narrowband gamma oscillation in mouse visual cortex. *Neuron*. 2017:93:315–322. https://doi.org/10.1016/j.neuron.2016.12.028.

Schmidt M, Bakker R, Shen K, Bezgin G, Diesmann M, van Albada SJ. A multi-scale layer-resolved spiking network model of resting state dynamics in macaque visual cortical areas. *PLoS Comput Biol*. 2018:14:e1006359. https://doi.org/https://doi.org/10.1371/journal.pcbi.1006359.

Schneider M, Broggini AC, Dann B, Tzanou A, Uran C, Sheshadri S, Scherberger H, Vinck M. A mechanism for inter-areal coherence through communication based on connectivity and oscillatory power. *Neuron*. 2021:109:4050–4067.e12. https://doi.org/10.1016/j.neuron.2021.09.037.

Self MW, Kooijmans RN, Super H, Lamme VA, Roelfsema PR. Different glutamate receptors convey feedforward and recurrent processing in macaque V1. *Proc Natl Acad Sci U S A*. 2012:109:11031–11036.

Self MW, van Kerkoerle T, Super H, Roelfsema PR. Distinct roles of the cortical layers of area V1 in figure-ground segregation. *Curr Biol*. 2013:23:2121–2129. https://doi.org/10.1016/j.cub.2013.09.013.

Self MW, Lorteije JAM, Vangeneugden J, van Beest EH, Grigore ME, Levelt CN, Heimel JA, Roelfsema PR. Orientation-tuned surround suppression in mouse visual cortex. *J Neurosci*. 2014:34(28):9290–9304. https://doi.org/10.1523/JNEUROSCI.5051-13.2014.

Smith MA, Jia X, Zandvakili A, Kohn A. Laminar dependence of neuronal correlations in visual cortex. *J Neurophysiol*. 2013:109:940–947. https://doi.org/10.1152/jn.00846.2012.

Song S, Sjöström PJ, Reigl M, Nelson S, Chklovskii DB. Highly nonrandom features of synaptic connectivity in local cortical circuits. *PLoS Biol*. 2005:3(3):e68. https://doi.org/10.1371/journal.pbio.0030068.

Storchi R, Bedford RA, Martial FP, Allen AE, Wynne J, Montemurro MA, Petersen RS, Lucas RJ. Modulation of fast narrowband oscillations in the mouse retina and dLGN according to background light intensity. *Neuron*. 2017:93:299–307. https://doi.org/10.1016/j.neuron.2016.12.027.

Tan AYY, Chen Y, Scholl B, Seidemann E, Priebe NJ. Sensory stimulation shifts visual cortex from synchronous to asynchronous states. *Nature*. 2014:509:226–229. https://doi.org/10.1038/nature13159.

Teramae J, Tsubo Y, Fukai T. Optimal spike-based communication in excitable networks with strong-sparse and weak-dense links. *Sci Rep*. 2012:2:485. https://doi.org/10.1038/srep00485.

Thomson AM, Morris OT. Selectivity in the inter-laminar connections made by neocortical neurons. *J Neurocytol*. 2002:31:239–246. https://doi.org/10.1023/A:1024117908539.

Thomson AM, West DC, Wang Y, Bannister AP. Synaptic connections and small circuits involving excitatory and inhibitory neurons in layers 2–5 of adult rat and cat neocortex: triple intracellular recordings and biocytin labelling in vitro. *Cereb Cortex*. 2002:12:936–953. https://doi.org/10.1093/cercor/12.9.936.

Uhlhaas PJ, Singer W. Abnormal neural oscillations and synchrony in schizophrenia. *Nat Rev Neurosci*. 2010:11(2):100–113. https://doi.org/10.1038/nrn2774.

Vaiceliunaite A, Erisken S, Franzen F, Katzner S, Busse L. Spatial integration in mouse primary visual cortex. *J Neurophysiol*. 2013:110(4):964–972. https://doi.org/10.1152/jn.00138.2013.

Van den Bergh T, Ziang B, Arckens L, Chino YM. Receptive-field properties of V1 and V2 neurons in mice and macaque monkeys. *J Comp Neurol*. 2010:518(11):2051–2070. https://doi.org/10.1002/cne.22321.

van Kerkoerle T, Self MW, Dagnino B, Gariel-Mathis M-A, Poort J, van der Togt C, Roelfsema PR. Alpha and gamma oscillations characterize feedback and feedforward processing in monkey visual cortex. *Proc Natl Acad Sci U S A*. 2014:111:14332–14341. https://doi.org/10.1073/pnas.1402773111.

Veit J, Hakim R, Jadi MP, Sejnowski TJ, Adesnik H. Cortical gamma band synchronization through somatostatin interneurons. *Nat Neurosci*. 2017:20:951–959. https://doi.org/10.1038/nn.4562.

Wagatsuma N, Potjans TC, Diesmann M, Fukai T. Layer-dependent attentional processing by top-down signals in a visual cortical microcircuit model. *Front Comput Neurosci*. 2011:5:31. https://doi.org/10.3389/fncom.2011.00031.

Wagatsuma N, Potjans TC, Diesmann M, Sakai K, Fukai T. Spatial and feature-based attention in a layered cortical microcircuit model. *PLoS One*. 2013:8:e80788. https://doi.org/10.1371/journal.pone.0080788.

Wagatsuma N, von der Heydt R, Niebur E. Spike synchrony generated by modulatory common input through NMDA-type synapses. *J Neurophysiol*. 2016:116:1418–1433. https://doi.org/10.1152/jn.01142.2015.

Wagatsuma N, Hu B, von der Heydt R, Niebur E. Analysis of spiking synchrony in visual cortex reveals distinct types of top-down modulation signals for spatial and object-based attention. *PLoS Comput Biol*. 2021:17(3):e1008829. https://doi.org/10.1371/journal.pcbi.1008829.

Wang XJ. Synaptic basis of cortical persistent activity: the importance of NMDA receptors to working memory. *J Neurosci*. 1999:19:9587–9603.

Wang XJ. Neurophysiological and computational principals of cortical rhythms in cognition. *Physiol Rev*. 2010:90:1196–1268. https://doi.org/10.1152/physrev.0035.2008.

Wang T, Li Y, Yang G, Dai W, Yang Y, Han C, Wang X, Zhang Y, Xing D. Laminar subnetworks of response suppression in macaque primary visual cortex. *J Neurosci*. 2020:40:7436–7450. https://doi.org/10.1523/JNEUROSCI.1129-20.2020.

Wilmes KA, Clopath C. Inhibitory microcircuits for top-down plasticity of sensory representations. *Nat Commun*. 2019:10:5055. https://doi.org/10.1038/s41467-019-12972-2.

Wilson NR, Runyan CA, Wang FL, Sur M. Division and subtraction by distinct cortical inhibitory networks in vivo. *Nature*. 2012:488:343–348. https://doi.org/10.1038/nature11347.

Womelsdorf T, Fries P, Mitra PP, Desimone R. Gamma-band synchronization in visual cortex predicts speed of change detection. *Nature*. 2006:439:733–736. https://doi.org/10.1038/nature04258.

Yatsenko D, Josić K, Ecker AS, Froudarakis E, Cotton RJ, Tolias AS. Improved estimation and interpretation of correlations in neural circuits. *PLoS Comput Biol*. 2015:11:e1004083. https://doi.org/10.1371/journal.pcbi.1004083.

Zhang S, Xu M, Kamigaki T, Hoang Do JP, Chang W-C, Jenvay S, Miyamichi K, Luo L, Dan Y. Long-range and local circuits for top-down modulation of visual cortex processing. *Science*. 2014:345:660–665. https://doi.org/10.1126/science.1254126.